LUNG BOUNDARY IDENTIFICATION AND COVID-19 CLASSIFICATION USING CT IMAGES BASED ON MACHINE LEARNING

2022
MASTER THESIS
COMPUTER ENGINEERING

Mustafa Kamil ABDULLAH

Thesis Advisor
Assist.Prof.Dr. Adnan Saher M. AL-AJEELI

LUNG BOUNDARY IDENTIFICATION AND COVID-19 CLASSIFICATION USING CT IMAGES BASED ON MACHINE LEARNING

Mustafa Kamil ABDULLAH

T.C.
Karabuk University
Institute of Graduate Programs
Department of Computer Engineering
Prepared as
Master Thesis

Thesis Advisor
Assist.Prof.Dr. Adnan Saher M. AL-AJEELI

KARABUK
August 2022

I certify that in my opinion the thesis submitted by Mustafa Kamil ABDULLAH titled "LUNG BOUNDARY IDENTIFICATION AND COVID-19 CLASSIFICATION USING CT IMAGES BASED ON MACHINE LEARNING" is fully adequate in scope and in quality as a thesis for the degree of Master of Computer Engineering.

Assist.Prof.Dr. Adnan Saher M. AL-AJEELI .....
Thesis Advisor, Department of Computer Engineering

This thesis is accepted by the examining committee with a unanimous vote in the Department of Computer Engineering as a Master of Science thesis. Aug 18 ,2022

Examining Committee Members (Institutions)	Signature
Chairman : Asst.Prof.Dr. Ferhat ATASOY (KBU)	.....
Member : Assist.Prof.Dr. Abdulkadir TAŞDELEN (AYBU)	.....
Member : Assist.Prof.Dr. Adnan Saher M. AL-AJEELI (KBU)	.....

The degree of Master of Science by the thesis submitted is approved by the Administrative Board of the Institute of Graduate Programs, Karabuk University.

Prof. Dr Hasan SOLMAZ .....
Director of the Institute of Graduate Programs

"I declare that all the information within this thesis has been gathered and presented in accordance with academic regulations and ethical principles and I have according to the requirements of these regulations and principles cited all those which do not originate in this work as well."

Mustafa Kamil ABDULLAH

ABSTRACT

M. Sc. Thesis

LUNG BOUNDARY IDENTIFICATION AND COVID-19 CLASSIFICATION USING CT IMAGES BASED ON MACHINE LEARNING

Mustafa Kamil ABDULLAH

Karabük University
Institute of Graduate Programs
The Department of Computer Engineering

Thesis Advisor:
Assist. Prof. Dr. Adnan Saher M. AL-AJEELI
August 2022, 54 pages

In early 2020, an existential health catastrophe result in the worldwide spread of the Coronavirus 2019 (COVID-19). Traditional healthcare strategies for treating COVID-19 may be improved with the use of automated CT imaging identification of lung infections as COVID-19. COVID-19 infection can only be diagnosed by using CT imaging. CT images are obtained from two databases: CC-CCII, MosMedData used for lung diagnosis classification (COVID-19 infections and normal). The significant heterogeneity and low density between infected and normal tissues make it difficult to identify infection using CT scans. The earlier COVID-19 infection predicate is used to perform a range of diagnostic activities, which helps identify pathological (COVID-19 infections) as well as enhances CT diagnostic reporting accuracy. Finally, modified machine learning models (CNN and SVM) were used to classify CT images as COVID-19 infection or normal. Analysis of experimental and clinical data shows that the proposed methodologies for examining the variability of the internal geometric

characteristics (lung diagnosis classification) of the lung and COVID-19 infections in images are effective. The modified systems showed that the accuracy of SVM with combined LBP with HOG is 98% and modified CNN of 98%.

Key Words : Image Processing, COVID-19 Infections, Classification, Feature Extraction, CT Image, Machine Learning.

Science Code : 92431

ÖZET

Yüksek Lisans Tezi

MAKİNE ÖĞRENİMİNE DAYALI CT GÖRÜNTÜLERİ KULLANARAK AKCİĞER SINIRLARININ TANIMLANMASI VE COVID-19 SINIFLANDIRMASI

Mustafa Kamil ABDULLAH

Karabük Üniversitesi
Lisansüstü Eğitim Enstitüsü
Bilgisayar Mühendisliği Anabilim Dalı

Tez Danışmanı:
Dr.Öğr.Üyesi. Adnan Saher M. AL-AJEELI
Ağustos 2022, 54 sayfa

2020'nin başlarında, bir sağlık felaketi, Coronavirus 2019'un (COVID-19) dünya çapında yayılmasına neden oldu. COVID-19'u tedavi etmeye yönelik geleneksel sağlık hizmetleri stratejileri, COVID-19 gibi akciğer enfeksiyonlarını tanımlamak için otomatik bilgisayarlı tomografi kullanılarak iyileştirilebilir. COVID-19 enfeksiyonu sadece bilgisayarlı tomografi (BT) kullanılarak teşhis edilebilir. BT görüntüleri, BT taramalarında COVID-19 akciğer anormalliklerinin sınıflandırılmasını iyileştirmek amacıyla kullanılan CC-CCII ve MosMedData olmak üzere iki veritabanından elde edilir. Enfekte doku ile normal doku arasındaki büyük heterojenlik ve düşük yoğunluk, BT taramaları kullanarak enfeksiyonu tanımlamayı zorlaştırır. Eski COVID-19 enfeksiyon verileri, hastalıkların (COVID-19 enfeksiyonu) belirlenmesine yardımcı olan ve ayrıca BT tanı raporlamasının doğruluğunu artıran bir dizi tanılama faaliyetini gerçekleştirmek için kullanılır. Son olarak, BT görüntülerini COVID-19 enfeksiyonu

veya normal olarak sınıflandırmak için değiştirilmiş makine öğrenme modelleri (CNN ve SVM) kullanıldı. Deneysel ve klinik verilerin analizi, görüntülerdeki akciğer iç geometrik özelliklerinin (sınıflandırma) ve COVID-19 enfeksiyonunun çeşitliliğini incelemek için önerilen metodolojilerin etkili olduğunu göstermektedir. Değiştirilmiş sistemler, HOG ile birleştirilmiş LBP ile SVM'nin doğruluğunun %98 ve değiştirilmiş CNN'nin %98 olduğunu göstermiştir.

Anahtar Kelimeler : Görüntü İşleme, COVID-19 Enfeksiyonları, Sınıflandırma, Özellik Çıkarma, BT Görüntüsü, Makine Öğrenme.

Bilim Kodu **:** 92431

ACKNOWLEDGMENT

I owe thanks and praise to God first and foremost for this success and facilitation as I bow to my beloved parents. My dear father gave me the most valuable things to make me a man of honor. My beloved mother is good at engineering my heart with her prayers. To my family that I grew up in and its extension gives me pride and honor. I owe a special thanks to my thesis supervisor, Assist. Prof. Dr. Adnan Saher M. ALAJEELI who spared no effort in providing unlimited advice and guidance until the completion of this thesis to the fullest.

I also extend my gratitude to Karabuk University, including the wonderful professors and colleagues who accompanied us throughout our academic journey, And i would like to thank my wife for supporting me throughout my studies.

I dedicate this thesis to my beloved country, Iraq. And to the beautiful Turkey, which embraced this scientific experience and contributed to providing all possibilities for graduating in this distinguished way.

CONTENTS

Page

Page

LIST OF FIGURES

Page

LIST OF TABLES

Page

PART 1

INTRODUCTION

On December 31, 2019, there was an epidemic of pneumonia in Wuhan, which is located in the province of Hubei, China. After being confirmed as a novel virus dubbed COVID-19, China officially disclosed the virus's genomic sequence on January 12th, 2020. On the 22nd of that month, proof of human-to-human transmission surfaced, and on the 30th, it was granted a worldwide high-risk status [1]. There seem to be 136,739,552 verified COVID-19 cases and 2,947,244 fatalities as of this posting (14 April 2021) ("WHO Coronavirus (COVID-19) Dashboard") World Health Organization [2]. As a result of the global lockdown measures, businesses were forced to modify or minimize their operations, which included restrictions on movement outside of the home and restrictions on maintaining brick-and-mortar retail outlets open [3-6].

An existential health disaster prompted the spread of initial 2020 global COVID-19. Automatic detection of lung diseases based on images generated by a CT scanner has a strong potential to enhance healthcare COVID-19 therapy method, and CT is crucial for diagnosis, assessment and initiation of COVID-19 infection. there are a number of issues with utilizing CT for COVID-19 detection, such as the strong contrast and low density between infected and healthy tissue [1,3].

1.1. RELEVANCE OF THE THESIS TOPIC

COVID-19 is a worldwide event that is still occurring, with a very recent start date and a highly unexpected nature due to the lack of previous encounters of such magnitude and scope in human history. It is also critical to investigate the complexities of its possible impact on other aspects of daily life in order to adjust to the new and

potentially long-term changes that the spread of sickness has forced on the public. Radiation diagnostics is a fast-evolving branch of medicine that incorporates artificial intelligence, computer vision, and novel medical imaging techniques.

The regency element is prominent in this research, given the topic's genesis date, since it could be one of the first research studies in the United Kingdom and what may be learned from it in the future. In the next part, I'd like to elaborate on the research's specific objectives [7].

In image identification and classification tasks, machine learning (ML) techniques, particularly deep learning, have made great progress. Many implementations in medical image analysis use computer methodologies ranging from deep neural networks to variational autoencoders, leading to their rapid growth [8,9]. Historically, in the diagnostic practice of radiology, physicians visually evaluate medical images to identify characteristics and monitor disease. The ability of machine learning and computer vision to recognize complicated patterns in imaging data and provide quantitative estimates of radiographic features [8,10,11] is impressive.

Based on the methods of ML, classification, and computer vision, significant advances have been made recently in the interpretation of sensory information, which makes it possible to better represent and interpret complex visual data. In [12], the main driving force behind ML and computer vision in medical imaging is the pursuit of greater efficiency and effectiveness in procedures for the clinical diagnosis of probable disease dynamics.

In comparison to the number of specialized radiologists, the large datasets linked to computed tomography continue to rise at a rapid pace. These factors are contributing to a significant rise in radiologists' workload. According to research, the radiologist, in certain situations, interprets the picture every 3-4 seconds during the course of an 8-hour workday in order to fulfill the demands of the hardware burden [9]. Accuracy is high in radiology since it involves both visual perception and decision-making under unpredictable settings, especially in a short time period.

1.2. THE MAIN PROBLEMS IN THE SUBJECT AREA

1. At the moment of the development of radiation diagnostics, it is not always possible to reliably formulate a conclusion about the identified zone of pathological changes (COVID-19, nodules, and tumors).
2. The problems can be found in a new branch of current medicine called "precision medicine," which tries to tailor treatment by considering the patient's and illness's unique qualities (having the condition or not) (having the disease or not).
3. A solution to the problem of inexperienced specialists, or the increase in patients' cases leads to a high rate of error in diagnosis, especially in villages and rural areas.

Because current radiation diagnosis is the most rapidly evolving field of instrumental medicine, there is a growing demand for more accurate and high-quality radiological results, for example, COVID-19 recognition. The amount of research carried out and the amount of information that needs to be processed by a specialist radiologist is especially growing as a result of the outbreak that is being caused by the COVID-19 coronavirus. Determination similarities of the revealed changes and a large amount of processed information are the main problems faced by the radiologist at the present time.

1.3. RESEARCH IDEA

Given the relevance of the COVID-19 problem, as well as the achievements of ML and computer vision in diagnostics, this study proposes the active use of a new technology for integrated processing and analysis of images - radionics, in the format of which a set of quantitative parameters of the investigated volumetric COVID-19 with the most accurate values of indicators.

1.4. THE AIM OF THE STUDY

The aim of the study is to improve the accuracy of geometric (morphological and texture) analysis and interpretation of images of lung pathology with COVID-19 to assess the corresponding indicators (highlighted area of infections as COVID-19 or normal) in the format of modern radionics technology.

To achieve the goal, the following tasks were formulated and solved:

1. using a database of images having pathological alterations in the lungs, including COVID-19 and normal.
2. Research and development of a computational for image interpretation and analysis (classification of lung diagnosis based on ML) that can identify complicated textural (morphological) forms quantitatively.
3. Analysis and interpretation of pathological alterations in COVID-19 patients, using a unique CT pattern.
4. Carrying out experimental studies to assess the effectiveness of the developed methodology within the framework of radionics technology.

1.5. SCIENTIFIC CONTRIBUTION OF RESEARCH

1. Methodology and algorithmic support for processing and analysis with increased accuracy of CT images with COVID-19.
2. Feature extraction of a segmented object with HOG and LBP in order to get higher accuracy of the infection class classification as (COVID-19, and Normal) based on machine learning (SVM), which allows analyzing the geometric (morphological and texture) features of CT images.
3. Modified CNNs model for COVID-19, and Normal classification.
4. The findings obtained from experimental researches based on the used database of CT images with COVID-19.

The scientific significance of the results of the task consists of combining the many aspects of the application of the theoretical foundations of radionics technology and the developed computational tools for geometric (morphological and textural,

segmentation COVID-19 changes, detection) analysis of CT images with Covid-19 to assess and control the involvement of the parenchyma of the affected lungs in the pathological process in order to plan therapy and predict the dynamics of changes to varying degrees.

1.6. ORGANIZATION OF THESIS

As mentioned earlier, the dissertation reviews and analyzes the techniques for lung tumor and COVID-19 infection detection. Additionally, the effectiveness of the techniques is analyzed and contrasted with the dataset. In Chapter 2, the new techniques in the field of classification (COVID-19 infections) are investigated. The research questions and research methodologies of this dissertation are explained in Chapter 3. Additionally, some literature and experiments are reviewed. Chapter 4 discusses the experiments and results. Conclusions and some future directions are then drawn in Chapter 5.

PART 2

LITERATURE REVIEW

COVID-19 is seen in patients using two imaging modalities. The use of chest radiography is one example. Several studies [13–15] have previously presented methods for categorizing them. In contrast, developing techniques using a sequence of operations is required for categorizing computed tomography (CT) scans. Infection clustering, infection identification, and volumetric measurement are all steps in the infection clustering and quantifying process [16,17].

Several studies on these methods may be found in the literature. It's worth noting that, because COVID-19 is a relatively novel disease, we still require tools that can conduct all of these duties simultaneously. In this part, we'll look at studies that look at how these techniques may be used together or independently for COVID-19 classification, infection identification, and change measurements.

2.1. CT SCAN (COMPUTED TOMOGRAPHY)

Computed tomography, or CT scanning, is a diagnostic technology that may help determine the cause of many medical problems. There are used a number of chest X-rays (CXR) and a supercomputer to construct a 3D image of sensitive tissue. CT scans, which are both painless and noninvasive, may be used by your doctor or other medical expert to identify disorders. A CT scan might be performed in a medical center or a separate imaging facility. Computed tomography, more often known as a CT scan, is used by medical professionals in order to examine the structures that are located inside your body. A CT scan uses CXR (chest X-ray) and software to produce images that show the interior of your body. It takes incredibly small "slices" of the bones, muscles, tissues, and plasma arteries to let healthcare professionals examine your body in great detail [18,19].

The term "conventional X-ray machines" refers to the types of X-ray equipment that use a stationary tube to focus the radiation on a specific area. As they go through the body, X-rays interact with a variety of tissues, each of which absorbs a different amount of the radiation. When placed against the dark background of the film, tissue with a greater density generates an image that is whiter than that of other tissues. X-rays produce images that are only in two dimensions. During a CT scan, an X-ray is rolled around in a doughnut-shaped tube that completely surrounds the patient. The data collected provides a detailed three-dimensional representation of the inside of your body, an example of CT scan device shown in Figure 2.1.

Figure 2.1. Patient entering CT scanner [18].

2.2. LUNG DIAGNOSIS OVERVIEW

Recently, CT, chest malignant neoplasms, and COVID-19 have become public health problems. According to the National Chest Screening Test (NCST), low-dose tomography (LDCT) Compared to radiography, it can cut deaths from lung cancer by 25% [20]. Diagnosis at an early stage is a crucial first step that greatly affects subsequent treatment options. Automatic determination of the boundaries of the lungs and affected areas (COVID-19) is really significant during the analyses and CT scans phase. It is a commonly used early diagnostic tool in clinical programs for the control of heart defects, including lung disease, heart disease, tumors, chest, pleural effusion,

edema, cardiac enlargement, and enlargement [21,22]. In some diagnostic cases, images directly related to the borders of the lungs, which can be extracted from a chest tomography, are used.

Tumor definition as well as classification for the Fleischer Association pictures of CT scans is “circular opacities with at least well-defined margins of no greater than 3 cm in diameter” [23]. Pattern recognition of medical images refers to dividing a digital image (scans) into multiple regions or collections of pixels. Every pixel in an area has specific or calculated characteristics such as color, density, or texture. Adjacent regions differ greatly in their similar characteristics [24].

In recent years, various analysts have proposed different techniques of CT scan’s segmentation, permitting to get the limits of the lungs. These strategies utilize various techniques. In this manner, methodological norms can be utilized, comprised of an arrangement including, but not limited to, procedures and guidelines, thresholds or morphological functions. Techniques dependence on this approach frequently have characteristic presumptions and ascertainable surmised arrangements. The results can be used to adjust the step to obtain more reliable (hash) segmentation algorithms [25]. Image processing techniques are used in chest x-rays (CXR) to determine the irregular size, size and shape of the lung. Chest CT images in the clinical evaluation are important in identifying lung disease [24]. A new deep lung infection screening network for COVID-19 (Inf-Net) has been proposed to automatically detect lesions in chest tomography [4].

The first phase in our effort to separate and extract bronchial tubes will be lung delineation, which is a critical step in an automated system. It will also be used to extract measurements since the area of the lung should be determined in order to establish the amount of lung participation. For numerous years, researchers have explored lung segmentation in CT [26,27]. To aid professionals in segmenting this organ, semi-automated and automatic approaches have been devised. Lung segmentation is an essential stage in image analysis that acts as a pre-processing phase for a number of later processes. It comprises, among other things, the identification of nodules, the identification of infected areas during radiotherapy, the segmentation of

changed lobes, and the extraction of coronary veins from the parenchyma [28]. According to 17-Wu, Y. H., et al. [29], lung delineation is a database difficulty rather than a methodological one. Furthermore, the authors claim that, although being published and established, lung segmentation algorithms still provide problematic outcomes in practical practice. The authors of this research conducted a large-scale analysis using various datasets and deep learning networks, as well as a comparison of two previous publications in the field.

The challenge of pixel-level predictions is addressed by object identification and segmentation. The purpose of semantic segmentation is to categorize each pixel's semantic label in a natural scan. For CT and x-ray image segmentation analysis, U-Net [30] is a commonly used machine learning.

Chandrashekar, G., et al. [31] did various tests to confirm the above-mentioned idea, demonstrating that different outcomes might be obtained based on different training datasets. Even when completing multiple trials, the accuracy of the dice coefficient [29] greater than 92.5 percent is always obtained. This shows that, despite using a different trained database to construct a segmentation method, it can produce substantial lung identification accuracy in a new database. As a result, there are no lung marks in the database. However, in order for the proposed approach to work better, the lungs needed to be segmented. To get trustworthy and accurate findings, researchers used a machine learning method on a segmentation issue, a large and diversified library, and different acquisition procedures. In [4,31], has yielded substantial results and may be utilized in clinical practice despite the lack of a measure to confirm the outcome in their foundation.

2.3. COVID-19 INFECTIONS DISEASE

Due to the fact that COVID-19 is a contemporary and global concern, work has accelerated on methods that can help professionals. However, it is vital to examine the characteristics that such a disease may display in CT scans in order to create computational approaches in radiography. In Refs. [13] The outline of the key features of COVID-19 infections. Ground-glass opacification is the most common imaging

anomaly, with infrequent aggregation in the periphery. Previously, certain viral segmentation techniques have been proposed.

In [32,33] suggested a novel machine learning method for infection localization. The author developed COVID-Seg-Net in order to better discriminate against infections. It is made up of a block of parameter variations. A huge research database with 21,758 CT scans was used in this work. When several samples are used for training, many photographs are extensively used for machine learning training, resulting in significant results. In infection segmentation, the authors' method gets a dice and a score of 72 percent.

Lung alterations caused by COVID-19 are mild in the beginning, occurring predominantly in the sub-pleural portions of one or maybe both lungs. Many lobes get engaged later in the disease, which causes a reduction of airflow and the consolidation of cancerous growths encircled by multiple B-lines. In respiratory failure (chest), particularly COVID-19 infection, an ultrasound scan reveals a whitish zone with no A-lines or separated B-lines. This type of appearance is referred to as a "white lung" [34,35].

The experiments were carried out using a database that had just 100 slices of CT scans, all of which were infected (database from [36]). Inf-Net received a dice and a score of 68.2 percent and 73.9 for Inf-Net. For infection segmentation, Zheng et al. [37] proposed a specified database collection procedure and the application of machine learning.

They used a developed lung segmentation method to partition the lungs and manually remove false positives. In a collection of 630 CTs, they employed a semi-supervised model named DeCovNet for infection separation. The 95.9% area curve was one of the outcomes. Wu et al. [29] have suggested a deep learning-based infection segmentation approach.

The approach is used on a consistent database [38] created specifically for the medical application, which contains 144,124 CT scans of more than 200 COVID-19 patients.

Joint classification and segmentation are the names of the networks that were employed (JCS). On COVID-19 identification, the approach had 95.0 percent sensitivity and 93.0 percent specificity, and 78.3 percent Dice on segmentation. When assessing the quantity of illness in the region, accuracy values of 93 percent at low resolution produce a substantial number of false positives [38]. They have developed an effective framework for lightweight multi-scale learning. The research is confined to 100 CT scans from individuals who have been diagnosed, yielding an average of 1.4 slices per subject (database available in [36]). Their approach yielded data with a sensitivity of 84.62 percent, a specificity of 96.42 percent, and a dice of 78.35 percent.

Qiu et al. [38] and Fan et al. [4] employed a 100-slice collection to demonstrate the capacity of deep learning approaches to provide results on such a tiny scale. In actual practice, however, a patient does not simply have 1.6 slices for each test, necessitating the categorization of an examination. However, there is some consistency in the database gathering process. Due to ethical constraints and incorrect diagnoses, among other considerations, it is not possible with all studies to acquire such a diverse set of data. As a result, segmenting infections is not an easy process, with a dice of 78.3 percent at best. However, we must keep an eye on the formation of false-positive in a segmentation approach for evaluating lung damage.

Wu et al. [29] discovered that improper classifications result in values of inappropriate dedication even with 78.3 percent Dice and a specificity of 93 percent. With 77.28 percent Dice and 97.42 percent specificity, Qiu et al. [38] discover the same thing. The current study [39] that a deep neural network was used with residual blocks to separate infections in CT, as well as a database created without using an acquisition technique that was based on the computational approach. Despite the fact that it is a tiny collection of the number of examinations (only 20 patients), it has almost 8000 slices. Lung segmentation and vascular segmentation are used for pathogen segmentation.

2.4. PATHOLOGY MEASUREMENT

The current work includes volumetric measurement of CT data in addition to infection detection. As a result, we give assistance to professionals for the monitoring, identification, and infection control of individuals suffering from this disease (COVID-19), which is claiming the lives of an increasing number of people every day. It's also important to quantify impairment when it comes to therapy. The lung's condition before and throughout therapy can help to demonstrate the treatment's efficacy and enhance the drug testing procedure [40,41].

According to work in [39], when types of deep begin to converge, a degradation problem emerges. Accuracy gets saturated (which may be predictable) as network depth increases, followed by a sharp decrease. Adding extra layers to a suitably deep model raises the training error, therefore overfitting cannot be to blame for this decline. As a result, He et al. [39] suggested using residual connections.

2.5. LUNG DIAGNOSIS CLASSIFICATION

Many studies have been published in journals [43–45] that use CXR (chest X-ray) and CT images [42] as a classification technique for COVID-19. CXR is less effective in the beginning stages, according to the researchers of Ref. [46], but a chest CT is required even before symptoms appear. One of the challenges with lung CT or CXR imaging is the likelihood of a diagnostic overlap between COVID-19, pneumonia, and lung disease. Other research, such as [24], focused on using lung datasets to identify and diagnose COVID-19. Furthermore, as demonstrated in references [47–50], several researchers used convolutional neural networks (CNN) with small datasets to identify and detect COVID-19 from lung X-ray images. In addition, as shown by Ref [33], several research have centered on detecting COVID-19 and classifying it as infected or normal.

Early COVID-19 identification early on assists in the separation of infected people and the avoidance of disease. Despite the fact that the Polymerase Chain Reaction (PCR) remains the primary and natural way of detecting COVID-19, some doctors are turning

to CT scans of the chest as a simpler, quicker, and more reliable method for diagnosing COVID-19. Early identification of COVID-19 may be aided by CT scanning. Because PCR test kits are in poor supply, a CT scan may be utilized as a last option to check for and detect Covid-19 [51]. Classification of the coronavirus (COVID-19) from X-ray and CT images is possible, although not using the same machine learning model [52]. The chest of individuals with COVID-19 shows anomalies such as ground glass, consolidation, and complete opacity on CT images [53]. The affected area became bigger and began to merge, resulting in the large-scale consolidation of some individuals in the advanced stage. Patients in the moderate or critical stage may have an extensive accumulation of the isolated or unilateral lungs, as well as ground-glass aperture settings and bronchial infection indications [54].

Because of its high transmissibility and fatality, the COVID-19 outbreak is classified as severe. The high number of people who need ICU hospitalization and long-term artificial breathing adds to the financial burden on the healthcare system [48]. Early detection is critical in this case for successful treatments and perhaps lowering stress in the public health system.

Artificial intelligence (AI)-based solutions may be able to deliver a low-cost and accurate diagnostic for COVID-19 and other kinds of pneumonia in this scenario [55]. Some studies [56,57] propose semi-supervised algorithms, which need some human intervention to achieve the desired outcomes. The authors method is totally automated, and it pulls infection-related indicators to aid professionals in addition to detecting diseases throughout a big database.

They developed a quick and effective method for recognizing COVID-19 instances using multitasking deep learning (DL) algorithms in this study [48]. The optimal approach is determined using X-ray and CT scans. COVID-19-infected areas were identified using a recurring Inception Deep Neural Network (IRDNN) with a Transfer Learning (TL) method, and COVID-19-infected regions were identified using a modified network model. The classification algorithm has an X-ray image testing accuracy of 84.67 percent and a CT image individual perception accuracy of 98.78 percent.

A multi-classification deep convolution method for recognizing COVID-19, pneumonia, and emphysema is suggested [45] using a mix of lung x-ray and CT images. Computed tomography (CT) may identify anomalies in the COVID-19 afflicted lungs, such as unilateral patchy blackness or Ground-Glass Opacity (GGO) as a non-invasive diagnostic technique [58,59]. As a result, CT may be an essential technique for early detection and diagnosis of individuals with COVID-19. Despite its benefits, CT imaging features may be similar to COVID-19, complicating automatic categorization. Even before symptoms appear, a chest CT scan is important in the early stages of sickness. A CT scan correctly identifies the anomalous attributes found in medical images. A CT scan can accurately detect the aberrant characteristics observed in medical images. The use of these two kinds of images will expand the dataset and improve classification accuracy [59].

CXR and CT scans provide crucial information for clinical diagnosis. By analyzing these images, we can create a machine learning approach for detecting viral outbreaks and identifying them. A two-stage data augmentation strategy can be used to classify medical scans from six different circumstances, including coronavirus images, in their study. because the dataset's scan count is insufficient and uneven. The second step of feature extraction is called synthetic minority excessively. Finally, the Principal Component Analysis (PCA) is decreased in size by eliminating associated features in the feature vector, using PCA methods. And, based on the data gathered, the proposed approach performs well, especially in terms of identifying COVID-19 quickly and effectively [31,60,61].

For invulnerable people, a CT scan is a useful technique for the detection of COVID-19 infection [62]. The predominant hallmark of the patients' lung CT is a ground-glass process more flexible with intermittent consolidation [6]. Treatment has become the key difficulty for physicians when the diagnosis is confirmed. There was no therapeutic strategy in place during the early days, so therapy was continued depending

on available medications. On May 1, 2020, the Food and Drug Administration consented to the usage of Remdesivir antiviral medications in adults and children with proven COVID-19 severe illness [63, 64]. This, however, isn't the end of the road.

To accurately diagnose classification model (COVID vs. Normal) and multi-class classification, advanced machine learning (ML) procedures can be applied in conjunction with radiological imaging. This can help to overcome the issue because there aren't enough trained doctors to serve outlying communities as well as to accurately detect this disease (COVID vs. Normal vs. Pneumonia). The generated classification has a 98.08% accuracy for binary classes and an 87.02% accuracy for multi-class situations. In our work, the DarkNet model served as a classifier for the YOLO real-time object identification system [95].

In [96], has been built a web app with all the features needed to submit a chest radiograph as input, analyze the picture, classify it, and then display the projected illness category, the class probability, and a link to download the auto-generated diagnostic report. After conducting image processing operations, the whole system comprises a CNN model that conducts categorization on input images. The CNN is trained with the use of a massive dataset of chest X-ray pictures, including those of patients with pneumonia and COVID-19, as well as healthy controls.

Following training to a wide range international cohort of 1280 patients to localize dorsolateral pleura/lung parenchyma, and then classifying cases of COVID-19 lung disease, a series of algorithms using deep learning has been shown in [97] to obtain up to 90.8% accuracy, when investigated using an independent dataset 1337 patients. Chest CTs performed for cancer, emergency, and pneumonia purposes were used as healthy controls. Among 140 patients with different (Non COVID -19) pneumonias verified in the lab, the false positive rate was 10%.

Remdesivir can reduce hospital stays; however, the virus manifests in a variety of ways, necessitating a variety of treatment options. A summary of machine learning approaches for lung and COVID-19 case identification and classification is provided in Table 2.1.

The neural network will help with the Covid-19 CT image identification scheme. This study evaluates lung disease classification methodologies using computed tomography using modified classifiers (CNN, SVM) on CT images to identify COVID-19 and normal lung based on characteristics extracted by (HOG and LBP) for improved accuracy.

Table 2.1. Summarizes studies that employed machine learning methods for lung and COVID-19 case.

NO	Study	Proposed Work	Methods	Medical Images	Performance	Disadvantage
1	(2020) [65]	Classification for COVID-19 vs. No-Findings, COVID-19 vs. Normal vs. Pneumonia)	Deep Neural Networks	Chest X-ray Images	98 Accuracy 87 Accuracy	Not showing the infected area as in left or right lung, size, and location
2	(2020) [28]	Classification for COVID vs. No COVID-19	Convolutional neural networks (CNNs)	CT scans	94 Accuracy	High false-positive rate of lung segmentation, difficult reagent transportation
3	(2020) [45]	detection of COVID-19	Deep Convolutional Neural Networks	Chest X-ray Images	98 Accuracy	Not showing the infected area as in left or right lung, size, and location
4	(2020) [66]	detection of COVID-19	The framework of Deep Learning	Chest X-ray Images	90 Accuracy	Time-consuming, Not showing the infected area as in left or right lung, size, and location
5	(2019) [42]	Multi-level COVID-19 Segmentation	Deep Network (Inf-Net)	CT scans	92 Accuracy	Need for matching instruments, low accuracy of low-level infections of COVID-19 segmentation
6	(2020) [48]	COVID-19 Segmentation	Multi-Task	Chest X-ray and CT Images	98 Accuracy	Cannot identify the type of other lung infections

			Deep Learning			
7	(2020) [22]	COVID-19 Segmentation and classification	Deep Learning	CT scans	96 Accuracy	Low throughput
8	(2020) [29]	COVID-19 Segmentation and classification	Convolutional Neural Networks (CNNs).	CT scans	88.63 Accuracy	Losing important part (infected area) of lung during the segmentation stage, and that will decrease the accuracy of classification or COVID 19 detection, requires large dataset for training and that will consume more time.
9	(2020) [24]	COVID-19 Segmentation and classification	Multi-task deep learning	CT scans	94 Accuracy	Time-consuming, Vulnerable to contamination
10	(2020) [4]	detection of COVID-19 vs. Normal vs. pneumonia	Deep Convolutional Neural Networks and Machine Learning	Chest X-ray Images	93 Accuracy	Low accuracy
11	(2020) [52]	COVID-19 detection	Deep Neural Networks (YOLO)	Chest X-ray Images	87 Accuracy	High false-positive rate; difficult reagent transportation
12	(2020) [41]	COVID-19 infection segmentation	Deep learning model	CT scans	78.3 Dice	High false-positive rate; difficult reagent transportation
13	(2022) [95]	COVID vs. Normal & COVID vs. Normal vs. Pneumonia	DNNs (YOLO)	X-ray chest	98.08 Accuracy 87.03 Accuracy	High false-positive rate on 3 classes, it means not detecting with high accuracy on multiclass,

						difficult reagent transportation

Although early research suggests that using chest CT for COVID-19 diagnosis and identification of infected regions might give promising results, currently, supervised learning, a methodology that is extensively used, forms the backbone of most methods. This needs a substantial amount of manual data labelling. However, in an epidemic, clinicians have very little time to finish the time-consuming hand sketching, putting the use of supervised deep learning algorithms in jeopardy. Using chest CT data from several facilities and scanners, we present an adjusted classification mechanism for areas infected with COVID-19. Based on detection data, we can also determine the diagnosis of COVID-19 patients.

Pandemics like the Coronavirus 2019 (COVID-19) outbreak in Wuhan, China, in 2019 are putting everyone's health at risk [67]. Around 82 percent of the time, COVID-19 causes minor symptoms, but it may potentially cause severe or even life-threatening symptoms in other circumstances. As of September 23, 2021, the World Health Organization (WHO) has verified COVID-19 in 229,373,963 people worldwide, with 4,705,111 fatalities [66, 68, 69]. On a global scale, diagnosed cases of COVID-19 are shown in Figure 2.2. SARS-CoV-2, the coronavirus has responsibility for the COVID-19 outbreak, is another name for the SARS-CoV-2 virus. The virus has survived in large numbers of infected people, although those with severe or critical conditions have died in fewer numbers. With an ever-growing COVID-19 infection rate, so does the need for critical care. If this trend continues in industrialized nations, it might lead to a collapse of the healthcare system. Congestion in intensive care units (ICUs) worsens the health of COVID-19 patients, who die at higher rates. X-rays and computed tomography scans are some of the tools used by researchers in their hunt for the new coronavirus' characteristics and symptoms [66,69]. Worldwide, the COVID-19 pandemic has cost billions of dollars in damage and slowed the development of the global economy significantly.

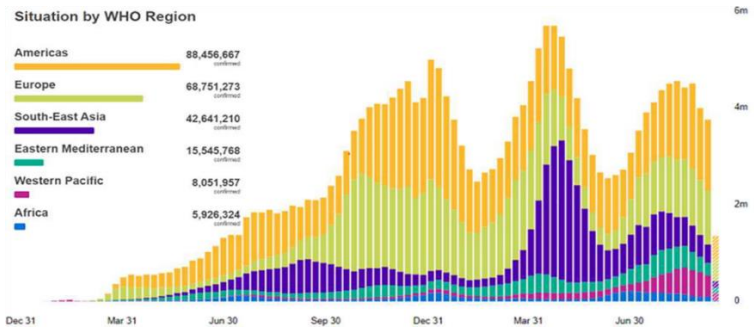

Figure 2.2. Distribution of COVID-19 cases worldwide until Sep. 2021 [68].

2.6. SYSTEM PERFORMANCE

These metrics were used to evaluate the efficacy of lung contour and nodule identification. Using the Pratt figure measurement (PFM), one may evaluate how similar two outlines are to one other.

$$PFM = \frac{1}{max(RE_{Cnt}, AE_{Cnt})} \cdot \sum_{i=1}^{1E_{Cnn}} \frac{1}{1 + \alpha \cdot d_i^2} \tag{2.1}$$

The positive class rate (also called the recall): Measurement of the right positive aspects' percentage is the goal here.

$$\text{Sensitivity } = \frac{TP}{TP + FN} \tag{2.2}$$

Indicates similar metrics by a coefficient of the Jaccard Similarity Index (JSI):

$$\Omega = \frac{TP}{TP + FP + FN} \tag{2.3}$$

In addition, the Dice Similarity Coefficient (DSC) can be used to assess the degree of overlap between two sets of data.

$$DSC = \frac{2 \cdot TP}{2 \cdot TP + FP + FN} \tag{2.4}$$

PART 3

THEORETICAL BACKGROUND

In the suggested study, classification methods were used to predict lung disease using CT scans. A CT scan of the lungs has shown a particular kind of lung disease. The use of computed tomography to classify and identify COVID-19 is a prominent focus of image processing. In order to build the COVID-19 detection model, preprocessing (image de-noising, methodologies, feature extraction, and classification) is based on the region of interest. The Support Vector Machine (SVM) and CNN are utilized in the classification stage. Figure 3.1 depicts the basis for utilizing CT scans to diagnose lung disease.

1. A CT scan of the lung collection.
2. Image converting to grayscale
3. Using histogram of oriented gradients (HOG) and Local binary patterns (LBP) transforms, for feature extraction on lung CT images for more accuracy of classification using SVM.
4. Training the models of 80 % of the database for training and 20% for testing.
5. Lung Classification in which the patient with COVID-19 or with a normal case using modified CNN for classification for earlier COVID-19 detection.
6. Data analysis.

Classification accuracy may be improved by comparing the lungs' extracted characteristics. In this work, all programs were implemented in the Python programming language. All methods were performed on the computer with Intel (R) Core (TM) i5 CPU and 8 GB RAM.

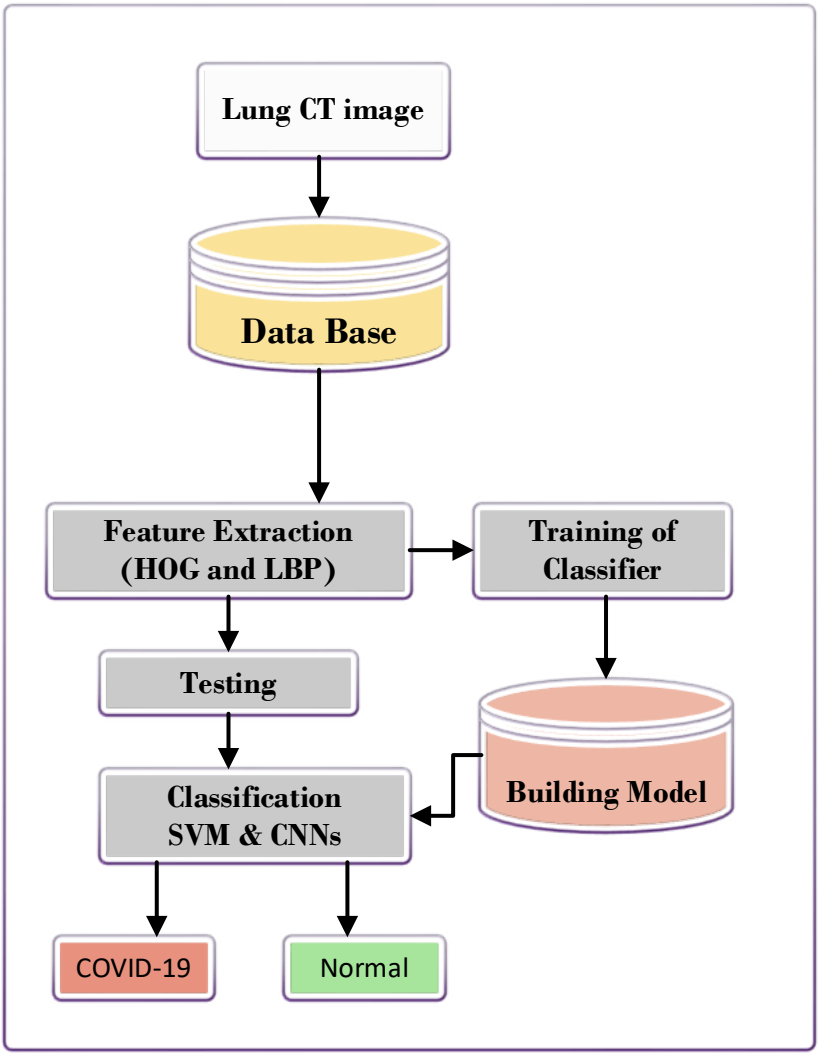

Figure 3.1. Framework of a model for the detection of lung disease using CT scan images.

3.1. CT IMAGE ENHANCEMENT

A grayscale image is a representation in which each pixel indicates the quantity of light or includes solely information about light intensity. It is a one-dimensional picture with just grayscale variations. As grayscale pictures are unidimensional, they are used to reduce the training complexity of models in a variety of applications and methods, including classification, object recognition, and prediction. There are four types of image conversion to grayscale in Python 3.6. 9 (Google Colaboratory environment performance) explained in Table 3.1.

Table 3.1. Functions of image convertors to grayscale in python.

No	Functions	Library
1	Image.convert ()	Pillow Library
2	Color.rgb2gray ()	Scikit-Image Module
3	cv2.COLOR_BGR2GRAY	OpenCV Library
4	Conversion Formula	Matplotlib Library

In our work we used third function of gray image conversion as :
Image_gray_original = cv2.cvtColor(image_original,cv2.COLOR_BGR2GRAY)

3.2. FEATURE EXTRACTION

Classification of lung CT images is a hard problem due to the diversity of infections as well as the severity of the infections that make the classification process very difficult. The process of classifying features has two stages: initially, features are extracted, and then the categorization of features that have been extracted. As a feature extractor, HOG and LBP descriptors were used. Both HOG and LBP are well known for being effective in extracting and representing image structure, patterns, and distinctive characteristics. In this work, we used LBP and HOG features separately. The proposed HOG and LBP features are extracted to train a classifier and enhance the classification accuracy. As classifiers, SVM and CNN are trained and used to classify the CT images.

3.2.1 Histogram Of Oriented Gradients Feature

To categorize patterns in images, object recognition algorithms employ the Histogram of Oriented Gradients (HOG). A medical image is analyzed to see how often each gradient's orientation occurs in a certain area. When it comes to extracting features, the HOG feature extraction module offers a quick and easy solution. It is a faster and more efficient feature descriptor than SIFT and LBP because of the fundamental computations [78]. HOG features have also been demonstrated to be useful as detection descriptors. Image processing and computer vision are two of the most

common uses of this technology. HOG may be used to describe the image's shape and appearance. The image is broken up into many individual cells, such as the 4-by-4 used in this research, and the edge directions are calculated this way. It is possible to normalize histograms in order to increase their accuracy.

In its most basic form, the HOG algorithm works by first dividing a picture into tiny squares cells, then computing a histogram of oriented gradients in each cell, then normalizing the result using a block-wise pattern, and finally returning a descriptor for each cell. The method has three main parameters: gradient orientation, cell size or pixels per cell, and cell per block.

The histogram of directional gradients' descriptor relies on the dispersion of intensity changes or data to characterize local object appearances and form. For each cell, a gradient direction histogram is created by dividing the picture into little linked pieces known as cells. In the next phase, they are use SVM to categorize the F-MNIST dataset's fashion items based on the extracted pictures' various attributes. It is necessary to do some preprocessing work prior to collecting image samples in order to remove noise artifacts before training a classifier and evaluating the test. Pre-processing results in better feature vectors for training classifiers. In order to reduce misclassification and improve identification rates, adequate preprocessing is essential. HOG-based feature extraction is used in the proposed study to identify fashion products. Images having a resolution of 2828 pixels are used to extract the HOG feature [79,80].

The descriptor is formed by integrating this information. Local histograms may make a significant improvement in accuracy by providing an estimate as a measure of the picture's overall intensity, common term for a group of cells, and then use this value to standardize each cell inside the group. This adjustment makes the reversal of bright and dark areas more effective. The steps of obtaining HOG features are shown in Figure 3.2.

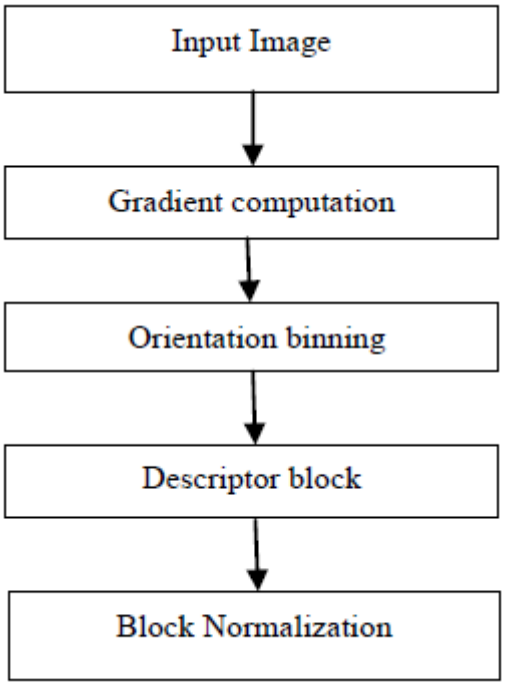

Figure 3.2. HOG feature extraction.

a) Gradient Computation

Each cell contains a 1-D distribution of gradient or border orientation over its pixels, gathered by breaking the picture window into small spatial parts known as cells. Throughout the process of calculating, the grade values are kept track of. The 1-D centered approach is the most often used technique, pointed discontinuous derivatives mask in both the horizontal and vertical axes. To create the gradients, we employed background subtraction and then tested them with a variety of discrete masking derivatives. Color or intensity data must be filtered to guarantee the efficacy of the kernels.

b) Orientation Binning

Calculating cells in statistical analysis is part of the next step in feature extraction. Edge direction histogram channel values are collected into orientation bins across tiny spatial regions called cells depending on how the focal gradational element is oriented

in space. There is a possibility that the forms might vary from square to spherical. When the gradients are signed, the rotation bins range from 0 to 360 degrees, but when they are unsigned, they only reach 0 to 180 degrees. When the gradients are unsigned, the rotation bins span from 0 to 180 degrees. For the range from 0 degrees to 180 degrees, the visual area is divided into 128 by 128 squares using a total of nine different direction bins. Each pixel's alignment is used to calculate the orientation bin that corresponds to it.

c) Descriptor Block

It is necessary to combine cells into larger, spatially connected blocks in order to alter the gradient strengths in the HOG features. Concatenation vectors of each region's modified cell scatter plots provide the HOG specification. In many cases, these blocks overlap, indicating that each cell is mentioned more than once in the final description. Both rectangular R-HOG and circular C-HOG blocks are examples of block geometric forms. In this experiment, the optimal settings for 2x2 holding cells of 4x4 pixel cells employing 9 percentile channels are calculated using the rectangular R-HOG. Each CT scan picture yields a total of 36 HOG feature sets.

d) Block Normalization

There are four main methods for doing block equalization. A small constant (e) is placed in front of V, which represents all the histograms in a given block, and the non-normalized vector V is used to represent all the histograms in this block (the exact value, hopefully, is unimportant). After that, you may choose an adjustment factor from the following list:

$$L2-normal:\ f=\frac{v}{\sqrt{||v||2+e^2}} \tag{3.1}$$

L2-hys: L2-normal followed by clipping (limiting the maximum values of v to 0.2) and renormalizing, as in

$$L2-normal:\ f=\frac{v}{||v||1+e} \tag{3.2}$$

$$L2-hys:\ f=\sqrt{\frac{v}{||v||1+e}} \tag{3.3}$$

Taking the L2-normal, compressing the outputs, and then renormalizing may be used to compute the L2-his method. On the other hand, the wide variances in the depth of field lead to a wide range of gradient magnitudes. To solve this problem, the histograms of each cell are normalized by combining neighboring cells into bigger blocks. Finally, the HOG-based bounding boxes are generated by joining all of the selected CT slices.

3.2.2. Local Binary Pattern Feature

As the title indicates, a Local Binary Pattern (LBP) describes an image's appearance in a small area around each pixel. Basic banalization was founded on the idea that textures convey two different local items: a pattern and the intensity of a pattern. A 3-pixel imaging block is used by the operator for local binary patterns. Thresholding is the value of the central pixel, which is then multiplied by powers of two, and then concatenated to give a label for this pixel. There are 28 = 256 possible labels that may be produced using the respective gray values of the middle and the pixels around the area since the neighborhood is made up of 8 pixels [79,81]. Additionally, when classifying images, the mean value and standard deviation of an image's LBP-local properties are taken into consideration. At the pixel level, LBPs transform a grayscale image into a matrix of numerical integers. This label matrix serves as a description of the original image. It does this by figuring out how to represent the texture on a map. CVs use this kind of graphic description as a way to group things. The performance is considerably enhanced when the HOG feature descriptors are employed.

A strong texture categorization characteristic, LBP is a feature descriptor. When interpreting CT images, it is critical to take texture into account. The LBP has been found to be a powerful extension for classification problems because of its invariance to grayscale and rotation [60]. The radius N surrounding the central pixel is what

determines the textural properties based on LBP sampling stations (neighborhood pixels) $LBP_{N,R}$:

$$LBP_{N,R}(x_c, y_c) = \sum_{k=0}^{N-1} s\big(x(k) - x(c)\big)2^k \quad , \qquad s(x) = \begin{cases} 1, x \geq 0 \\ 0, x < 0, \end{cases} \tag{3.4}$$

Where R is the circle's radius and N is the number of sample points at that radius. LBP pixel density is controlled by R, which governs the quantization of angular space. As a consequence, the accuracy of classification is strongly influenced by these two factors. X (K) the values of the pixel K and x(C) denote the values of the center pixel C, The function s guarantees that LBP's gray-scale and rotation invariants are invariant (x). In this case, s(x) has a value of 1 if it is larger or equal to the value of the pixel x (K). Otherwise, s(x) has a value of 0.

3.3. FEATURE FUSION

Feature fusion is a method of combining two or more descriptors to enhance the learning and classification method. It is used mostly with image processing applications. The approach combines or concatenates features from different branches. To our knowledge, the feature fusion method for combining HOG and LBP descriptors has not been utilized by any other researcher. This is the highest motivation to explore this approach and investigate its results. As we know, the HOG descriptor focuses on extracting shape information (i.e., edge information). On the other hand, LBP is focused on extracting texture information. So, combining these two descriptors will give us a very powerful tool to classify any kind of image. The combining procedure is also affecting the results. There are several feature fusion methods in the literature. The most common way of combining features is through summation or concatenation. In the summation method, two or more features wanted to be combined are put into one vector. The resultant vector will start with one feature and continue to the next in a serial manner. In this work, we used concatenation, in which we simply concatenate one feature vector to the other. This kind of combination makes certain that no information is lost during the procedure.

3.4. CLASSIFICATION

Image classification is a supervised learning issue, which means that need to first specify a collection of target classes (things that need to be identified in images), and then train a model to recognize them using labeled sample photographs. Raw pixel data served as the primary input for the early computer vision models that were developed. Picture classification is an essential endeavor that seeks to get an understanding of an image in its entirety as a whole. The objective is to label the picture so that it may be filed away in the appropriate category. In most cases, when people talk about image classification, they are referring to the analysis of photographs in which there is just one item visible. Item detection, on the other hand, is a method that analyzes more realistic scenarios in which an image may include more than one object. This method requires both classification and localization tasks to be completed.

3.4.1 Support Vector Machine (SVM)

The SVM uses a purely statistical method to determine which of two possible outcomes will be selected. where an SVM training technique is given a set of examples separated into two categories and then constructs a model that assigns new instances to one of the two groups. Hyperplanes and hyperplane sets are generated by support vector machines for classification applications in a high dimension or infinite dimension space. When used with machine learning to uncover patterns in data, SVMs are an efficient supervised learning method. It is possible to get to the hyperbolic plane if one achieves a sufficient amount of separation and the largest possible distance from neighboring training data in every category. A larger margin of error will help lessen generalization errors. The maximum boundary classifier is shown in Figure 3.3. SVM is a classification and regression classifier, are widely employed in supervised learning [82]. For example, face recognition, word recognition, and so on may all benefit from using the Supporting Vector Machine. When used in real-world scenarios, it delivers excellent results [83]. Using SVM, we trained and tested this classification on medical images. Using a multiclass SVM classifier, the F-MNIST database's fashion photographs were classified in HOG feature space using this approach. HOG features

of 1296 x 1296 have been arranged in rows to fill the whole feature area. The diagram of the SVM classifier is shown in Figure 3.3.

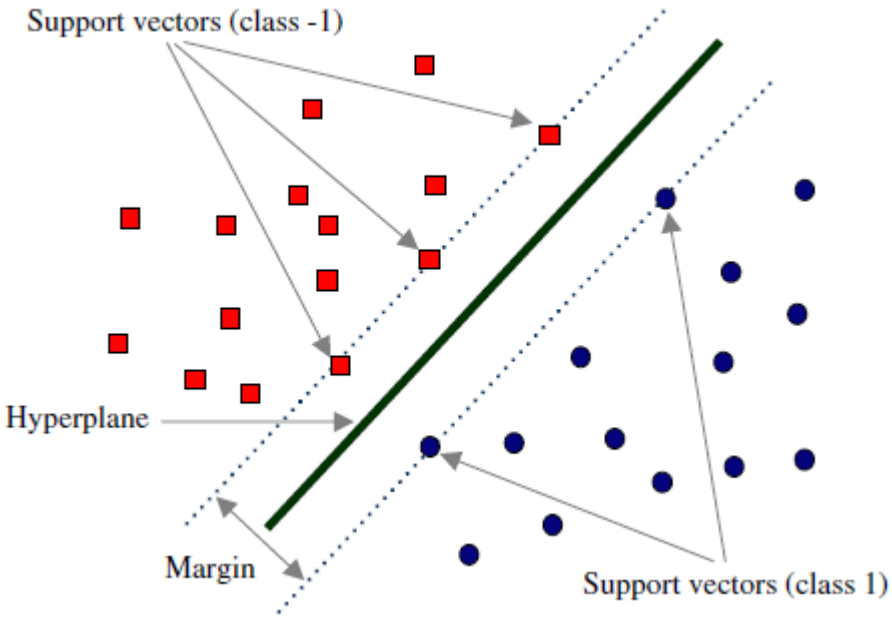

Figure 3.3. Maximal margin classifier.

3.4.1.1. Multi-Class SVM

Rather of creating a large number of binary classifiers, it makes more sense to do a single optimization technique to separate all of the categories [84]. All k-binary SVMs may be learned at the same time using these techniques, which offer a clear goal variable and maximize offsets from each category to the remaining items for a k-class problem. Assuming a labeled training set, $\{(x_1, y_1), \ldots . (x_n, y_n)\}$ of cardinality l, where $x\_i \in R\text{^}d \; and \; y\_i \in \{1, \ldots, k\}$, the formulation used in [85] is given as follows:

$$\min \frac{1}{2} \sum_{m=1}^{k} W_m^T W_m + C \sum_{i=1}^{1} \sum_{t \neq y_i}, \qquad (3.5)$$

$$W_m \in H, b \in R^k, א \in R^{lxk}$$

subject to $W_{y_i}^T \varphi(x_i) + b_{y_i} \geq W_t^T \varphi(x_i) + b_t + 2 - \aleph_{i,t}$ (3.6)

$$i = 1, \ldots, l, t \in \{1, \ldots, k\} \setminus y_i.$$

The result of the decision is:

$$\arg \_max_m f_m(x) = \arg_{max\ m} (W_M^T \varphi(x) + b_m) \quad (3.7)$$

3.4.2. Modified CNN Model

In our study, we noticed a difficulty in detecting images with fine features. as opposed to being really complex like ResNets or ResNext [60] models, the model that is doing such classification should have a structure that can detect and learn from slight differences. An instance of the suggested model employed in this work is provided in Figure 3.4. The suggested model contains four convolution layers. for this purpose, we use a batch normalization approach that, in addition to standardizing the inputs, also offers a number of other benefits, like reducing necessary training time and improving model stability. LeakyReLU is a modification of the ReLU method used to save cells from death. In each of the pooling processes, the Maxpool method is the one that is carried out. When Maxpool receives an input, it takes the maximum value from the region specified by the filter and reduces the size of the input. When there are two different classes involved, the suggested model accomplishes the COVID-19 and normal classification jobs. CT scans may be classified as either COVID-19 or Normal using the same model regardless of whether three different types of input images are used. Figure 3.5 presents, as a final step, the model's layer details as well as the layer parameters for each layer. The deep learning model that was created has a total of 1,050,226 parameters. The Adam optimizer was used for weight updates, the cross entropy loss function, and selected learning.

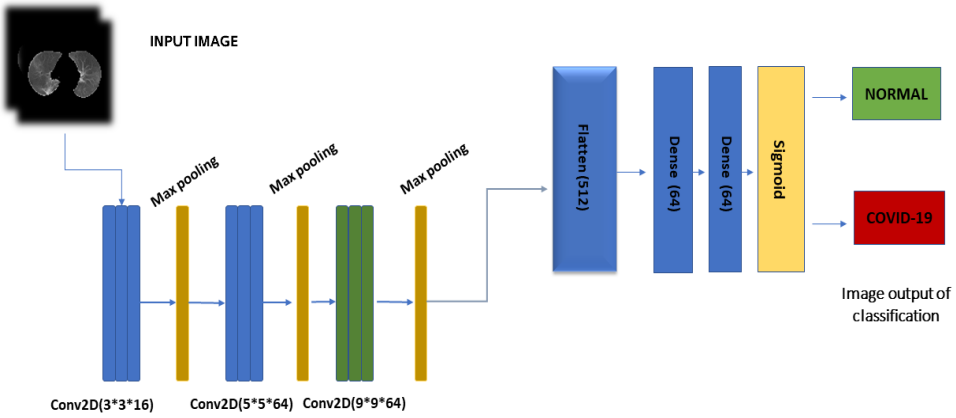

Figure 3.4. Modified CNN model.

Layer (type)	Output Shape	Param #
conv2d_6 (Conv2D)	(None, 254, 254, 16)	448
max_pooling2d_6 (MaxPooling 2D)	(None, 127, 127, 16)	0
conv2d_7 (Conv2D)	(None, 123, 123, 16)	6416
max_pooling2d_7 (MaxPooling 2D)	(None, 61, 61, 16)	0
conv2d_8 (Conv2D)	(None, 53, 53, 16)	20752
max_pooling2d_8 (MaxPooling 2D)	(None, 26, 26, 16)	0
flatten_2 (Flatten)	(None, 10816)	0
dense_4 (Dense)	(None, 64)	692288
dense_5 (Dense)	(None, 2)	130

Total params: 720,034
Trainable params: 720,034
Non-trainable params: 0

Figure 3.5. Model summary.

We've chosen CNN's design using one of the following hypotheses: COVID-19 or normal (no infection). The purpose of this is to assist radiologists in prioritizing COVID-19 patients for PCR testing and treating infections based on their unique etiology. With these needs in mind, we created the CNN-CT architecture, which comprises of three parallel layers with 16, 64, and 64 filters in each layer, all of which are different sizes (3-by3, 5-by-5, and 9-by-9). The coevolved pictures are then subjected to batch normalization and rectified linear unit, followed by two types of pooling operations: both average and maximum pooling. The rationale for employing different filter sizes is to identify local features with 3-by-3 filters and somewhat global features with 9-by-9 filters, while the 5-by-5 filter size is used to pick up the details that the other two filters overlook.

PART 4

METHODOLOGY

4.1. EXPERIMENTS AND RESULTS

In the study's experiment section, experiments using a computed tomography image database were used to examine lung illnesses associated with COVID-19 (lung classification as person with COVID-19 or with normal case). For COVID-19 diagnosis classification, we used two databases of CT scans. The first is china's National Chest CT Image Database (CC-CCII) (China) and this globally available dataset has been used by [29]. The second is MosMedDat was provided by Moscow's municipal hospitals, Russia [88], the images in second dataset has been selected for images that have all lung, due some images not having whole part of lung, finally that will effect for extracted features on lung, example is shown in Figure 4.1. The calculated outcomes and the efficiency of the suggested method were analyzed were obtained to assess lung extraction associated with COVID-19 and classification (CT scan with COVID-19 or normal). Table 4.1 shows the summary of used databases.

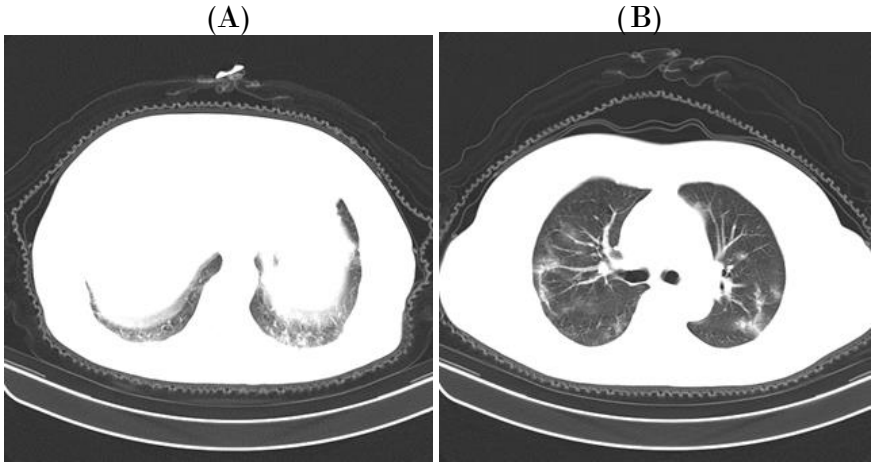

Figure 4.1. Example of MosMedDat images of the same patient.

Table 4.1. An exhaustive synopsis of the study's data.

DATASET	ORIGIN		DESCRIPTION		AVAILABLE AT:
The CC-CCII Dataset, Created By the China Consortium for Chest CT Image Research	❖ Sun Yat-sen Memorial Hospital and Third Affiliated Hospital of Sun Yat-sen University, Guangzhou, China ❖ The first Affiliated Hospital of Anhui Medical University, Anhui, China ❖ West China Hospital, Sichuan, China ❖ Nanjing Renmin Hospital, Nanjing, China ❖ Yichang Central ❖ People's Hospital, Hubei, China ❖ Renmin Hospital of Wuhan University, Wuhan, China	Patients	Scans	Label	http://ncov-ai.big.ac.cn/download
		929	1544	COVID-19 Positive	
		964	1556	Common Pneumonia (Negative)	
		849	1078	Normal Lung (negative)	
MosMedData	Municipal hospitals in Moscow, Russia	150	408	COVID-19 (positive)	https://mosmed.ai
		100	253	Normal lung (negative)	

Figure 4.2. shows an examples of CT images from China Consortium of Chest CT Image Investigation (CC-CCII) Dataset, the CC-CCII dataset contains segmented lung of all CT images (Normal and COVID-19).

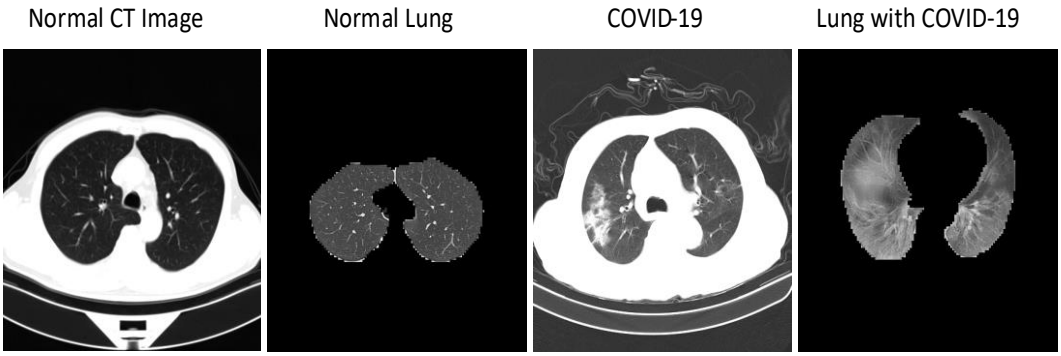

Figure 4.2. Example of CC-CCII dataset.

Figure 4.3. Shows an examples of CT images from Municipal hospitals in Moscow, Russia, which is called MosMedData, this dataset includes only CT images of normal and COVID-19, and thier segmented method applied on MosMedData for lung extraction for classification [88].

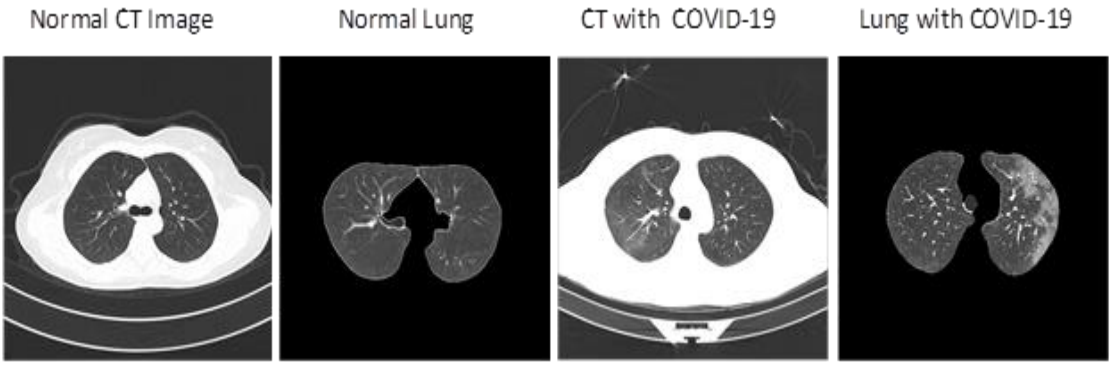

Figure 4.3. Example of MosMedData images with the segmented lung[88].

The classification has been performed on the CT images and segmented lung with diffident datasets.

4.2. LUNG CLASSIFICATION

Classification of lung segment is a hard problem, due to the diversity of infections as well as the severity of the infections that make the classification process very difficult. The process of classifying features has two stages: initially, features are extracted, and then the categorization of features that have been extracted. As a feature extractor Histogram of the Gradient feature descriptor (HOG) and Local Binary Pattern (LBP) was used. Both HOG and LBP are well known for being effective in extracting and representing image structure, patterns, and distinctive characteristics. In this work besides using LBP and HOG features separately, a novel method called feature fusion was utilized. The proposed feature fusion method combines two different features extracted to train a classifier and enhance the classification accuracy. As a classifier, SVM and CNN are trained and used to classification of the CT images and segmented lungs.

One kind of supervised learning model is the support vector machine (SVM). This learning model is used labeled data to train and predict. SVM is proven to be a very robust and effective prediction classifier and is used in many research areas. SVM is widely used in image processing applications and in medical image classification due to the successful results that are present. That is the biggest motivation for using an SVM classifier in this work.

HOG basically divides a picture into tiny squares cells, provides a description for each cell after computing a histogram of oriented gradients in each cell and normalizing the result using a block-wise pattern. Generally speaking, the approach has three primary settings: gradient direction, cell size (in pixels), and pixels per cell, and cell per block.

The experimental results of the HOG with SVM classifier are shown in Table 4.2. After several experiments, when the orientation parameter is set to 9 the accuracy improved. therefore we could say that when orientation = 9, the HOG descriptor is best fit to the characteristics of the dataset and CT images in general. In the rest of this work, the orientation parameter should be assumed 9. The other two parameters' effects on the accuracy result are seen in Table 4.2. It can be seen that when the cell

size is equal to 8x8, the results are very promising regardless of the block size. We can say that the model mainly depends on cell size, not the block size, and the best results are obtained when the cell size is set to 8x8. In the rest of this research, we chose HOG parameters as follows: orientation = 9, cell size = 8x8, block size = 4x4.

Table 4.2. Results of HOG descriptor with SVM classifier in lung infections.

Dataset	**Training Images**	**Testing Images**	**PARAMETERS**		**ACCURACY (HOG with SVM)**
			Cell Size (pixels)	**Block Size (cells)**	
MosMedData	2541	619	**8 x 8**	**4 x 4**	**0.9632**
			4x4	4x4	0.9421
			4x4	8x8	0.8656

Local binary pattern is a simple yet very effective method to extract texture information from images. Primary applications include pattern recognition and texture categorization. It has also been proven that it is a good feature extractor for many other applications, like medical image analysis. Since the structure of CT images has textured shapes, LBP is a useful method for this kind of problem. LBP is using a threshold to obtain features from each pixel, comparing or using data from neighbor pixel the threshold operation utilizes a binary image as the resultant image.

There are only two parameters used in this approach, radius and N points. An input image's pixels are surrounded by their neighbors, and the radius parameter determines the radius of those neighbors, while N points is the number of neighbors used to compute the descriptor.

The results of LBP features with the SVM classifier are shown in Table 4.3. It can be seen that decreasing radius and N point’s parameters are increasing the accuracy of detection also, but when increasing radius and N point’s parameters are decreasing the accuracy but at the cost of computation time. Based on the outcomes of experiments introduced in Table 4.3, we can say that the best result is obtained when radius = 2 and N points = 16.

Table 4.3. Results of LBP descriptor with SVM classifier in lung infections.

Dataset	Training Images	Testing Images	Radius	N points	ACCURACY (LBP with SVM)
MosMedData	2541	619	**2**	**16**	**0.9685**
			3	24	0.9015
			4	32	0.9035
			8	64	0.9195

4.3. RESULTS OF COMBINING (LBP & HOG) WITH SVM CLASSIFIER

Based on the experimental results introduced, results of feature fusion (HOG + LBP) with SVM classifier in lung infection (COVID-19) classification are shown. From Table 4.4, we can recognize that the best results of classification are when the cell size is 8x8 or block size is 4x4, radius 2, and N points is 16, which the accuracy is 98.07 %.

Table 4.4. Results of feature fusion (HOG + LBP) with SVM in lung infections.

Dataset	Training Images	Testing Images	PARAMETERS				ACCURACY
			Cell Size (pixels)	Block Size (cells)	Radius	N points	
MosMedData	2541	619	4x4	4x4	3	24	0.8254
			8 x 8	**4 x 4**	**2**	**16**	**0.9807**
			4x4	8x8	8	64	0.7687
			4x4	4x4	4	32	0.9065

From Table 4.4, we can recognize that the best results of classification are when the cell size is 8x8, block size 4x4, radius 2, and N points is 16, which the accuracy is 98.07 %.

The analysis and classification of COVID-19 and normal on CC-CCII and MosMedData database has been used with the modified CNN, The details shown in Table 4.5.

Table 4.5. The evaluation of modified CNNs model on different database.

With Segmented Lung				
Dataset	**Training Images**	**Testing Images**	**Loss Test**	**Accuracy Test**
CC-CCII	5878	157	0.0128	**0.9862**
MosMedData	2541	560	0.2978	**0.9756**
With CT images (Without Lung segmentation)				
Dataset	**Training Images**	**Testing Images**	**Loss Test**	**Accuracy Test**
MosMedData	2541	619	0.5613	**0.9696**

As shown in Table 4.5, the classification of COVID-19 and normal on CC-CCII and MosMedData database has been used the modified CNN. We can recognize that the accuracy of images with segmented lung is more accuracy than images without lung segmentation, The test accuracy of COVID-19 and normal classification using modified CNN is 0.9862, and the loss test is 0.0128 on the CC-CCII, while the accuracy test on the MosMedData database is 0.9756, and 0.9696 with segmented lung and without segmentation respectively, and the loss test is 0.2978 and 0.5613. Therefore, that the lung segmentation increased the classification of test accuracy and decreased the loss test on MosMedData database. The final matrices of model performance using precision, recall, and F1-Score are shown in Table 4.6.

Table 4.6. Evaluation performance of COVID-19 and normal classification.

With Segmented Lung					
Dataset	**Training Images**	**Testing Images**	**Precision**	**Recall**	**F1-Score**
CC-CCII	5878	157	1.00	0.94	0.97
Average			0.98	0.96	0.97
MosMedData	2541	560	0.92	0.99	0.95
Average			0.95	0.93	0.94
With CT images (Without Lung segmentation)					
MosMedData	2541	572	1.00	0.95	0.97
Average			0.98	0.97	0.97

Compared to human experts and the work of the ML system [29] for accurate diagnosis, COVID-19 infection detection, and prognosis of COVID-19 pneumonia using computed tomography, our methodology archived a high accuracy of classification as shown in Table 4.7 and calculated confusion matrix in Figure 4.4.

Table 4.7. Compactions of performance evaluation with other research work.

Reference	**Database**	**Model**	**Accuracy %**	**F1-Score %**
[29], 2020	CC-CCII	3D CNN model DenseNet3D121	88.63	88.14
[29], 2020	CC-CCII	3D CNN model ResNet3D34	87.83	86.04
Our first model	**CC-CCII**	**Modified CNN**	**98.62**	**97.00**
[94], 2020	Xray-COVID19	LBP plus SVM	93.04	-
[94], 2020	Xray-COVID19	HOG plus SVM	88.05	-
Our second model	**MosMedData**	**Hybrid SVM**	**98.07**	**-**

As shown in our study, the modified CNN classifier was used with the CC-CCII data and the accuracy was (98.62) and compared to the work of this study [29] that used

the same data (CC-CCII) with the CNN classifier as shown in Table 4.7 and the accuracy was (88.63) and from this we conclude that our modified CNN classifier had the highest classification accuracy.

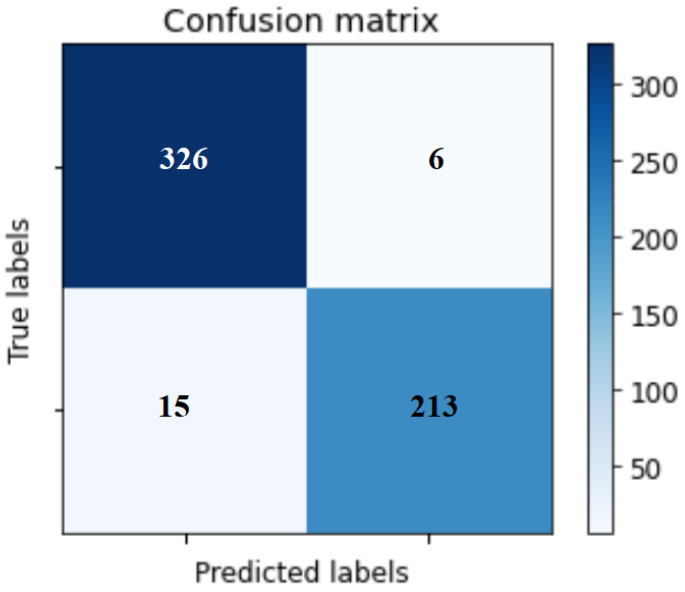

Figure 4.4. Calculated confusion matrix on CC-CCII database using modified CNN.

When using another dataset, MosMedData, with the classifier SVM, when the descriptors (HOG + LBP) were combined with SVM, we got (0.9807) as shown in Table 4.4 and and calculated confusion matrix in Figure 4.5.

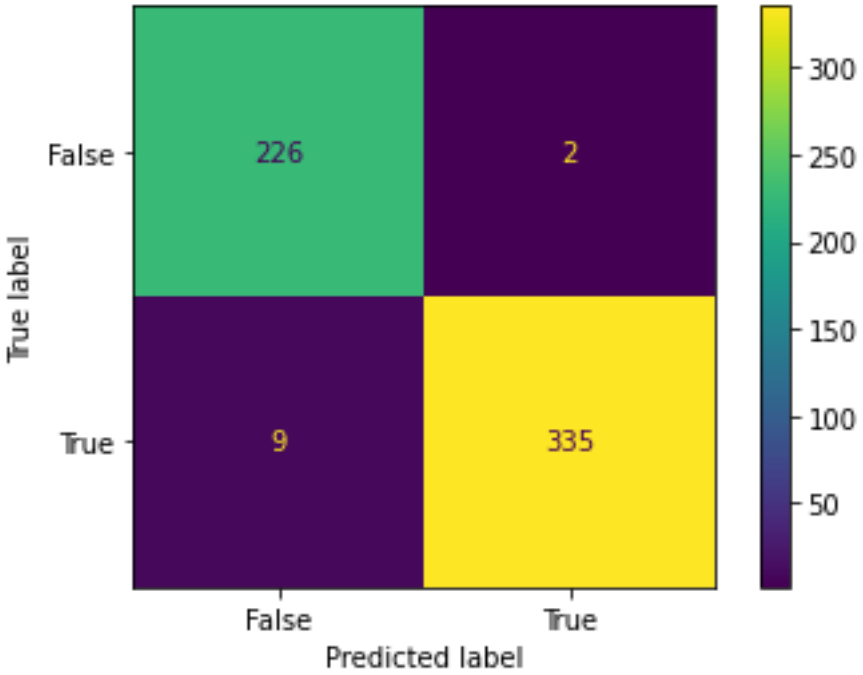

Figure 4.5. Calculated confusion matrix on MosMedData database using SVM.

On the other hand, we utilized the same data (MosMedData) with the CNN classifier, which gave classification accuracy (0.9696).

Due to the use of the proposed method for feature fusion of the HOG+ LBP features together, it gave us good feature extraction, which led to obtaining a higher accuracy in classification.

PART 5

CONCLUSION

The data used in this study about the coronavirus includes information from the European Centre for Disease Prevention and Control and the World Health Organization, a European Union agency, and other official websites around the world. CT images are obtained from two databases: CC-CCII and MosMedData and are used for lung diagnosis classification (COVID-19 infections and normal).

The modified approach for coronavirus (COVID-19) identification utilizing CT scans and segmented lung is based on two machine learning models: deep features and CNN, and LPB and HOG features with SVM. We did this by extracting the deep feature pre-trained CNN model and giving it to CNN, LPB, and HOG, each with its own SVM classifier. Each classification model is run five times, and the average result is recorded to improve the robustness of the classification model. When compared to other classification models, the CNN with segmented lung classification model performed better. On the CC-CCII, the used classification model (CNN) for COVID-19 detection achieved an accuracy test of 0.9862 and a loss test of 0.0128; on the MosMedData database, the accuracy test is 0.9756 and 0.9696 with segmented lung and without segmentation, respectively, and the loss test is 0.2978 and 0.5613 before and after lung segmentation. As a result, using CT images with segmented lungs increased the accuracy of classification and reduced test loss in the MosMedData database. The SVM classifier, on the other hand, achieved 0.9807 by combining LPB and HOG features and cell sizes of 4x4 and block sizes of 8x8. A huge dataset might be used to expand this thesis. This approach has a drawback if the patient is in a life-threatening scenario and unable to undergo CT scanning.

REFERENCES

1. S. Zhao, Q. Lin, J. Ran, S. Musa, "Preliminary estimation of the basic reproduction number of novel coronavirus (2019-nCoV) in China, from 2019 to 2020: A data-driven analysis in the early", ***G. Y.-I. journal of, and undefined 2020*** Elsevier,Accessed:Jan.06,2022

2. Z. Ye, Y. Zhang, Y. Wang, Z. Huang, and B. Song, "Chest CT manifestations of new coronavirus disease 2019 (COVID-19): a pictorial review", ***European Radiology***, vol. 30, no. 8, pp. 4381–4389, Aug. 2020, doi: 10.1007/S00330-020-06801-0.

3. J. Yang et al., "Prevalence of comorbidities in the novel Wuhan coronavirus (COVID-19) infection: a systematic review and meta-analysis", ***covid-19.conacyt.mx***, Accessed: Jan. 06, 2022.

4. D. Fan, T. Zhou, et al. "Inf-net: Automatic covid-19 lung infection segmentation from CT images", ***IEEE Transactions on Medical Imaging*** 39.8 (2020): 2626-2637.

5. Nie, D., Gao, Y., Wang, L., and Shen, D., "ASDNet: Attention Based Semi-Supervised Deep Networks for Medical Image Segmentation", Lecture Notes in Computer Science (Including Subseries Lecture Notes in Artificial Intelligence and Lecture Notes in Bioinformatics), ***Springer International Publishing***, 370–378 (2018).

6. M. Y. Ng et al., "Imaging profile of the covid-19 infection: Radiologic findings and literature review", ***Radiology: Cardiothoracic Imaging***, vol. 2, no. 1, Feb. 2020, doi: 10.1148/RYCT.2020200034.

7. B. Vlačić, L. Corbo, L., e Silva, S. C., & Dabić, M. (2021). "The evolving role of artificial intelligence in marketing A review and research agenda", ***Journal of Business Research***, 128, 187-203.

8. Litjens, G., Kooi, T., Bejnordi, B. E., Setio, A. A. A., Ciompi, F., Ghafoorian, M., ... & Sánchez, C. I. (2017). "A survey on deep learning in medical image analysis", Medical image analysis, 42, 60-88, **https://doi.org/10.1016/j.media.2017.07.005**

9. Santos, M. K., Ferreira, J. R., Wada, D. T., Tenório, A. P. M., Barbosa, M. H. N., & Marques, P. M. D. A. (2019). "Artificial intelligence, machine learning, computer-aided diagnosis, and radiomics: advances in imaging towards to precision medicine", ***Radiologia brasileira***, 52, 387-396.

10. S. Chan and E. L. Siegel, “Will machine learning end the viability of radiology as a thriving medical specialty ? ”, ***British Journal of Radiology***, vol. 92, no. 1094, 2019, doi: 10.1259/BJR.20180416.

11. Giger, M. L. (2018). “Machine learning in medical imaging”. ***Journal of the American College of Radiology***, 15(3), 512-520.

12. P. Dorado-Díaz, … J. S.-G.-R. E., and undefined 2019, “Applications of artificial intelligence in cardiology. The future is already here”, Elsevier, Accessed:Jan.01,2022, **https://doi.org/10.1016/j.rec.2019.05.014 (2019)**.

13. Aljondi, R., & Alghamdi, S. (2020). “Diagnostic value of imaging modalities for COVID-19: scoping review”, ***Journal of medical Internet research***, 22(8), e19673.

14. M. Ahsan, K. Gupta, M. Islam, … S. S.-M. L. and, and undefined 2020, “Covid-19 symptoms detection based on nasnetmobile with explainable ai using various imaging modalities”, ***mdpi.com***, Accessed: Dec. 16, 2021.

15. Y. Yang, Y. Huang, F. Gao, L. Yuan, Z. W.-I. C. Medicine, and undefined 2020, “Lung ultrasonography versus chest CT in COVID-19 pneumonia: a two-centered retrospective comparison study from China”, ***Springer***, vol. 46, pp. 1761–1763, 2020, doi: 10.1007/s00134-020-06096-1.

16. M. Kiran, I. Ahmed, N. Khan, and A. G. Reddy, “Chest X-ray segmentation using Sauvola thresholding and Gaussian derivatives responses”, ***Journal of Ambient Intelligence and Humanized Computing***, vol. 10, no. 10, pp. 4179–4195, Oct. 2019, doi: 10.1007/S12652-019-01281-7.

17. A. M. Zaki, S. van Boheemen, T. M. Bestebroer, A. D. M. E. Osterhaus, and R. A. M. Fouchier, “Isolation of a Novel Coronavirus from a Man with Pneumonia in Saudi Arabia”, ***New England Journal of Medicine***, vol. 367, no. 19, pp. 1814–1820, Nov. 2012, doi: 10.1056/NEJMOA1211721.

18. J. Ashi, “11. COMPUTED TOMOGRAPHY SCAN IMAGE ANALYSIS OF SEDIMENTS1”, ***Scientific Results***, vol. 156, 1997, Accessed: Dec. 16, 2021.

19. Kirsch, T. D., Hsieh, Y. H., Horana, L., Holtzclaw, S. G., Silverman, M., & Chanmugam, A. (2011). “Computed tomography scan utilization in emergency departments: a multi-state analysis”, ***The Journal of emergency medicine***, 41(3), 302-309.

20. T. Blanchon, J. Bréchot, P. Grenier, G. F.-L. cancer, and undefined 2007, “Baseline results of the Depiscan study: a French randomized pilot trial of lung cancer screening comparing low dose CT scan (LDCT) and chest X-ray (CXR)”, Accessed:Dec.16,2021, Elsevier, **https://doi.org/10.1016/j.lungcan.2007.05.009**

21. J. Pu et al., “Automated quantification of COVID-19 severity and progression using chest CT images”, ***European Radiology***, vol. 31, no. 1, pp. 436–446, Jan. 2021, doi: 10.1007/S00330-020-07156-2.

22. S. Hu et al., “Weakly supervised deep learning for covid-19 infection detection and classification from ct images”, **ieeexplore.ieee.org**, Accessed: Dec. 16, 2021.

23. Y. Hamad, M. Seno, … M. A.-K.-… of E. and, and undefined 2021, “Segmentation and measurement of lung pathological changes for COVID-19 diagnosis based on computed tomography”, **pen.ius.edu.ba**, Accessed: Dec. 16, 2021.

24. A. Amyar, R. Modzelewski, H. Li, S. R.-C. in B. and, and undefined 2020, “Multi-task deep learning based CT imaging analysis for COVID-19 pneumonia: Classification and segmentation”, Elsevier, Accessed: Dec. 16, 2021, **https://doi.org/10.1016/j.compbiomed.2020.104037**

25. X. Pan et al., “Accurate segmentation of nuclei in pathological images via sparse reconstruction and deep convolutional networks”, Elsevier, Accessed: Dec. 16, 2021, **https://doi.org/10.1016/j.neucom.2016.08.103**

26. D. Müller, I. S. Rey, and F. Kramer, “Automated Chest CT Image Segmentation of COVID-19 Lung Infection based on 3D U-Net”, Jun. 2020, Accessed: Dec. 16, 2021, **https://doi.org/10.48550/arXiv.2007.04774**

27. M. Abdel-Basset, V. Chang, … H. H.-K.-B., and undefined 2021, “FSS-2019-nCov: A deep learning architecture for semi-supervised few-shot segmentation of COVID-19 infection”, Elsevier, Accessed: Dec. 16, 2021, **https://doi.org/10.1016/j.knosys.2020.106647**

28. M. I.-B. S. P. and Control and undefined 2021, “Automatic diagnosis of coronavirus (COVID-19) using shape and texture characteristics extracted from X-Ray and CT-Scan images”, Elsevier, Accessed: Dec. 16, 2021, **https://doi.org/10.1016/j.bspc.2021.102602**

29. He, X., Wang, S., Shi, S., Chu, X., Tang, J., Liu, X., ... & Ding, G. (2020). “Benchmarking deep learning models and automated model design for COVID-19 detection with chest CT scans”, **MedRxiv**.

30. M. Alom, C. Yakopcic, … M. H.-J. of M., and undefined 2019, “Recurrent residual U-Net for medical image segmentation”, **spiedigitallibrary.org**, Accessed:Dec.16,2021.

31. Chandrashekar, G., & Sahin, F. (2014). “A survey on feature selection methods. Computers & Electrical Engineering”, 40(1), 16-28, **https://doi.org/10.1016/j.compeleceng.2013.11.024**

32. Q. Yan, B. Wang, D. Gong, C. Luo, … W. Z. preprint arXiv, and undefined 2020, “COVID-19 chest CT image segmentation--a deep convolutional neural network solution”, **arxiv.org**, Accessed: Dec. 16, 2021.

33. R. Lokwani, A. Gaikwad, V. Kulkarni, … A. P. preprint arXiv, and undefined 2020, “Automated detection of covid-19 from ct scans using convolutional neural networks”, **arxiv.org**, Accessed: Dec. 16, 2021.

34. Larici, A. R., Cicchetti, G., Marano, R., Merlino, B., Elia, L., Calandriello, L., ... & Natale, L. (2020). “Multimodality imaging of COVID-19 pneumonia: from diagnosis to follow-up. A comprehensive review”, ***European journal of radiology***, 131, 109217.

35. L. Sultan, C. S.-U. in M. & Biology, and undefined 2020, “A review of early experience in lung ultrasound in the diagnosis and management of COVID-19,” Elsevier,Accessed:Dec.16,2021, **https://doi.org/10.1016/j.ultrasmedbio.2020.05.012**

36. “COVID-19 - Medical segmentation”, (accessed Dec. 16, 2021), **http://medicalsegmentation.com/covid19**

37. C. Zheng et al., “Deep learning-based detection for COVID-19 from chest CT using weak label”, **medrxiv.org**, doi: 10.1101/2020.03.12.20027185.

38. Qiu, Y., Liu, Y., Li, S., & Xu, J. (2021, May). “Miniseg: An extremely minimum network for efficient covid-19 segmentation”, ***In Proceedings of the AAAI Conference on Artificial Intelligence*** (Vol. 35, No. 6, pp. 4846-4854).

39. K. He, X. Zhang, S. Ren, J. S.-P. of the IEEE, and undefined 2016, “Deep residual learning for image recognition”, **openaccess.thecvf.com**, Accessed: Dec. 16,2021.

40. M. Petrou, L. E. Quint, B. Nan, and L. H. Baker, “Pulmonary nodule volumetric measurement variability as a function of CT slice thickness and nodule morphology”, In ***American Journal of Roentgenology***, vol. 188, no. 2, pp. 306–312, Feb. 2007, doi: 10.2214/AJR.05.1063.

41. K. Men, J. Dai, Y. L.-M. physics, and undefined 2017, “Automatic segmentation of the clinical target volume and organs at risk in the planning CT for rectal cancer using deep dilated convolutional neural networks”, In ***Wiley Online Library***, vol. 44, no. 12, pp. 6377–6389, Dec. 2017, doi: 10.1002/mp.12602.

42. Kim, H. H., Jo, J. H., Teng, Z., & Kang, D. J. (2019). “Text detection with deep neural network system based on overlapped labels and a hierarchical segmentation of feature maps”, In ***International Journal of Control***, Automation and Systems, 17(6), 1599-1610.

43. Ding, J., Li, A., Hu, Z., & Wang, L. (2017, September). “Accurate pulmonary nodule detection in computed tomography images using deep convolutional neural networks”, In ***International Conference on Medical Image Computing and Computer-Assisted Intervention,*** (pp. 559-567). Springer, Cham.

44. Stull, K. E., Tise, M. L., Ali, Z., & Fowler, D. R. (2014). “Accuracy and reliability of measurements obtained from computed tomography 3D volume rendered images”, In ***Forensic science international***, 238, 133-140.

45. A. N.-2020 M. T. C. (TIPTEKNO) and undefined 2020, “Detection of Covid-19 Patients with Convolutional Neural Network Based Features on Multi-class X-ray Chest Images” , In **ieeexplore.ieee.org**, Accessed: Dec. 16, 2021.

46. R. Pereira, D. Bertolini, L. Teixeira, … C. S. J.-C. M. and, and undefined 2020, “COVID-19 identification in chest X-ray images on flat and hierarchical classification scenarios,” Elsevier, Accessed: Dec. 16, 2021, In **https://doi.org/10.1016/j.cmpb.2020.105532**

47. S. Asif, Y. Wenhui, H. Jin, S. J.-2020 I. 6th International, and undefined 2020, “Classification of COVID-19 from Chest X-ray images using Deep Convolutional Neural Network” , In **ieeexplore.ieee.org**, Accessed: Dec. 16, 2021.

48. M. Alom, M. Rahman, M. Nasrin, … T. T. preprint arXiv, and undefined 2020, “COVID_MTNet: COVID-19 detection with multi-task deep learning approaches” , In **arxiv.org**,Accessed:Dec.16,2021.

49. Wang, L., Lin, Z. Q., and Wong, A., "COVID-Net: a tailored deep convolutional neural network design for detection of COVID-19 cases from chest X-ray images", ***Scientific Reports***, 10 (1): 1–12 (2020).

50. A. S. Al-Waisy et al., “COVID-CheXNet: hybrid deep learning framework for identifying COVID-19 virus in chest X-rays images”, In ***Soft Computing***, 2020, doi: 10.1007/S00500-020-05424-3.

51. A. Abbas, … M. A.-I. T. on, and undefined 2021, "4S-DT: Self-Supervised Super Sample Decomposition for Transfer Learning With Application to COVID-19 Detection", In **ieeexplore.ieee.org**, Accessed: Dec. 16, 2021.

52. Ş. Öztürk, U. Özkaya, M. B.-I. J. of, and undefined 2021, "Classification of Coronavirus (COVID-19) from X-ray and CT images using shrunken features", In ***Wiley Online Library***, vol. 31, no. 1, pp. 5–15, Mar. 2020, doi: 10.1002/ima.22469.

53. S. Moosavi, … A. M.-T. I., and undefined 2020, "COVID-19 clinical manifestations and treatment strategies among solid-organ recipients: a systematic review of cases," In ***Wiley Online Library***, vol. 22, no. 6, Dec. 2020, doi: 10.1111/tid.13427.

54. K. L. Shen et al., "Updated diagnosis, treatment and prevention of COVID-19 in children: experts' consensus statement (condensed version of the second edition)", In ***World Journal of Pediatrics***, vol. 16, no. 3, pp. 232–239, Jun. 2020, doi: 10.1007/S12519-020-00362-4.

55. Y. Shang et al., "Management of critically ill patients with COVID-19 in ICU: statement from front-line intensive care experts in Wuhan, China", In ***Annals of Intensive Care***, vol. 10, no. 1, Dec. 2020, doi: 10.1186/S13613-020-00689-1.

56. J. O. B. Diniz et al., "Segmentation and quantification of COVID-19 infections in CT using pulmonary vessels extraction and deep learning", In ***Multimedia Tools and Applications***, vol. 80, no. 19, pp. 29367–29399, Aug. 2021, doi: 10.1007/S11042-021-11153-Y.

57. A. Haidar and L. Holloway, "Integration of Deep and Ensemble Learning for Detecting COVID-19 in Computed Tomography Images", 2020, doi: 10.21203/rs.3.rs-82263/v2, In **https://www.researchsquare.com/article/rs-82263/v2**

58. M. Zhou, X. Zhang, and J. Qu, "Coronavirus disease 2019 (COVID-19): a clinical update", In ***Frontiers of Medicine***, vol. 14, no. 2, pp. 126–135, Apr. 2020, doi: 10.1007/S11684-020-0767-8.

59. D. Wang et al., "Clinical characteristics of 138 hospitalized patients with 2019 novel coronavirus–infected pneumonia in Wuhan, China", In **jamanetwork.com**, Accessed:Dec.16,2021.

60. E. P.-I. Journal and undefined 2016, "Texture feature extraction by using local binary pattern", In **jurnal.informatika.lipi.go.id**, Accessed: Jan. 06, 2022.

61. S. Rueda, C. Knight, A. P.-M. image analysis, and undefined 2015, “Feature-based fuzzy connectedness segmentation of ultrasound images with an object completion step”, Elsevier, In ***Medical Image Analysis***, Accessed: Jan. 06, 2022.

62. T. Ai et al., “Correlation of Chest CT and RT-PCR Testing for Coronavirus Disease 2019 (COVID-19) in China: A Report of 1014 Cases”, Radiology, vol. 296, no. 2, pp. E32–E40, Aug. 2020, In **https://pubs.rsna.org/doi/10.1148/radiol.2020200642**

63. Mann, G. J. Use of Remdesivir in COVID-19”, In **credencemedicure.com**, Accessed:Dec.16,2021.

64. E. Hillaker, J. Belfer, A. Bondici, … H. M.-… : T. J. of, and undefined 2020, “Delayed initiation of remdesivir in a COVID-19-positive patient”, In ***Wiley Online Library***, vol. 40, no. 6, pp. 592–598, Jun. 2020, doi: 10.1002/phar.2403.

65. T. Ozturk, M. Talo, E. Yildirim, … U. B.-C. in biology, and undefined 2020, “Automated detection of COVID-19 cases using deep neural networks with X-ray images”, Elsevier, In ***Computers in Biology and Medicine***, Accessed: Dec. 16, 2021.

66. E. E.-D. Hemdan, M. A. Shouman, and M. E. Karar, “COVIDX-Net: A Framework of Deep Learning Classifiers to Diagnose COVID-19 in X-Ray Images”, In **https://arxiv.org**. 2020, Accessed: Jan. 06, 2022.

67. A. Atangana and S. İğret Araz, “Mathematical model of COVID-19 spread in Turkey and South Africa: theory, methods, and applications”, In ***Advances in Difference Equations***, vol. 2020, no. 1, Dec. 2020, doi: 10.1186/S13662-020-03095-W.

68. “COVID-19 vaccines: everything you need to know | Gavi, the Vaccine Alliance”, In **https://www.gavi.org/covid19** (accessed Jan. 06, 2022).

69. A. S. Al-Waisy et al., “COVID-CheXNet: hybrid deep learning framework for identifying COVID-19 virus in chest X-rays images”, In ***Soft Computing***, 2020, doi: 10.1007/S00500-020-05424-3.

70. Z. Zhang, D. Han, J. Dezert, Y. Y.-S. processing, and undefined 2018, “A new adaptive switching median filter for impulse noise reduction with pre-detection based on evidential reasoning”, Elsevier, Accessed: Jan. 06, 2022, In **https://doi.org/10.1016/j.sigpro.2018.01.027**

71. Z. Huang, X. Wang, J. Wang, … W. L.-P. of the, and undefined 2018, “Weakly-supervised semantic segmentation network with deep seeded region growing”, In **openaccess.thecvf.com**, Accessed: Jan. 06, 2022.

72. D. Zeebaree, … H. H.-… on A. S., and undefined 2019, “Machine learning and region growing for breast cancer segmentation”, In **ieeexplore.ieee.org**, Accessed: Jan.06,2022.

73. A. Isaac, H. Khanna Nehemiah, and A. Kannan, “Computer-Aided Diagnosis System for Diagnosis of Cavitary and Miliary Tuberculosis Using Improved Artificial Bee Colony Optimization”, In ***IETE Journal of Research***, 2021, doi: 10.1080/03772063.2021.1946440.

74. S. Lou, L. Pagani, W. Zeng, X. Jiang, P. S. engineering, and undefined 2020, “Watershed segmentation of topographical features on freeform surfaces and its application to additively manufactured surfaces”, Elsevier, In ***Precision Engineering,*** Accessed: Jan. 06, 2022.

75. Heinrich, M. P., & Blendowski, M. (2016, October). “Multi-organ segmentation using vantage point forests and binary context features”, In ***International Conference on Medical Image Computing and Computer-Assisted Intervention,*** (pp. 598-606). Springer, Cham.

76. X. Yang et al., “Cardiac image segmentation by random walks with dynamic shape constraint”, In ***IET Computer Vision***, vol. 10, no. 1, pp. 79–86, Feb. 2016, doi: 10.1049/iet-cvi.2014.0450.

77. Chakraborty, S. and Mali, K., "A morphology-based radiological image segmentation approach for efficient screening of COVID-19", ***Biomedical Signal Processing And Control***, 69 (May): 102800 (2021).

78. Z. Xiang, H. Tan, W. Y.-I. Access, and undefined 2018, “The excellent properties of a dense grid-based HOG feature on face recognition compared to Gabor and LBP”, **ieeexplore.ieee.org**, Accessed: Jan. 06, 2022.

79. W. Zhou, S. Gao, L. Zhang, X. L.-I. T. on Circuits, and undefined 2020, “Histogram of oriented gradients feature extraction from raw bayer pattern images”, **ieeexplore.ieee.org**, Accessed: Jan. 06, 2022.

80. K. Greeshma, K. S.-I. J. of Innovative, and undefined 2019, “Fashion-MNIST classification based on HOG feature descriptor using SVM”, **researchgate.net**, Accessed:Jan.06,2022.

81. T. Tuncer, S. Dogan, F. O.-C. and I. Laboratory, and undefined 2020, "An automated residual exemplar local binary pattern and iterative ReliefF based COVID-19 detection method using chest X-ray image," Elsevier, In ***(2020) Chemometrics and Intelligent Laboratory Systems,*** Accessed: Jan. 06,2022.

82. Konstantinidis, D., Stathaki, T., Argyriou, V., & Grammalidis, N. (2016). Building detection using enhanced HOG–LBP features and region refinement processes. In ***IEEE Journal of Selected topics in applied Earth observations and Remote Sensing***, 10(3), 888-905.

83. J. Yang, Z. Chen, J. Zhang, C. Zhang, Q. Zhou, and J. Yang, "HOG and SVM algorithm based on vehicle model recognition", In ***MIPPR (2019) Pattern Recognition and Computer Vision***, p. 44, Feb. 2020, doi: 10.1117/12.2538191.

84. al Jinkun Yang et al., "HOG and SVM algorithm based on vehicle model recognition," **spiedigitallibrary.org**, p. 44, Feb. 2020, doi: 10.1117/12.2538191.

85. A. Krishan, D. M.-T. C. Journal, and undefined 2021, "Multi-Class Liver Cancer Diseases Classification Using CT Images", In ***(2021) The Computer Journal***, Accessed: Jan. 06, 2022.

86. World Health Organization. (2020). addressing human rights as key to the COVID-19: response, 21 April 2020 (No. WHO/2019-nCoV/SRH/Rights/2020.1). In ***World Health Organization***.

87. He, X., Wang, S., Shi, S., Chu, X., Tang, J., Liu, X., ... & Ding, G. (2020). Benchmarking deep learning models and automated model design for COVID-19 detection with chest CT scans. **MedRxiv**.

88. Morozov, S. P., Andreychenko, A. E., Pavlov, N. A., Vladzymyrskyy, A. V., Ledikhova, N. V., Gombolevskiy, V. A., ... & Chernina, V. Y. (2020). Mosmeddata: Chest ct scans with covid-19 related findings dataset. ***arXiv preprint arXiv***:2005.06465.

89. Zhou, T., Canu, S., & Ruan, S. (2020). An automatic COVID-19 CT segmentation based on U-Net with an attention mechanism. In ***(2021) International Journal of Imaging Systems and Technology***, 2004.06673.

90. Ming-Yen, N., YP, L. E., Jin, Y., Fangfang, Y., Xia, L., and Hongxia, W., "Imaging Profile of the COVID-19 Infection: Radiologic Findings and Literature Review", ***Radiology: Cardiothoracic Imaging***, 2 (1): 1–8 (2020).

91. Zhang, K., Liu, X., Shen, J., Li, Z., Sang, Y., Wu, X., ... & Wang, G. (2020). Clinically applicable AI system for accurate diagnosis, quantitative measurements, and prognosis of COVID-19 pneumonia using computed tomography. In ***Cell,*** 181(6), 1423-1433.

92. Zhao, J., Zhang, Y., He, X., & Xie, P. (2020). COVID-CT-Dataset: a CT scan dataset about COVID-19, In ***(2020) arXiv preprint arXiv***, 2003.13865.

93. Elharrouss, O., Subramanian, N., & Al-Maadeed, S. (2020). An encoder-decoder-based method for covid-19 lung infection segmentation, In ***(2020) arXiv preprint arXiv***, 2007.00861.

94. P. Kumar Sethy, S. Kumari Behera, P. Kumar Ratha, and P. Biswas, "Detection of coronavirus Disease (COVID-19) based on Deep Features and Support Vector Machine," 2020, **www.preprints.org**

95. Aboughazala, L. M. (2020). Automated detection of COVID-19 coronavirus cases using deep neural networks with X-ray images. In ***Al-Azhar University Journal of Virus Researches and Studies***, 2(1), 1-12.

96. Harmon, S. A., Sanford, T. H., Xu, S., Turkbey, E. B., Roth, H., Xu, Z., ... & Turkbey, B. (2020). Artificial intelligence for the detection of COVID-19 pneumonia on chest CT using multinational datasets, from ***Nature communications***, 11(1), 1-7.

97. Mehta, S. C. M. R. S., & Sharma, P. (2021). Covid-19 and Pneumonia Chest Infection Detection and Classification using Convolutional Neural Networks. In ***Turkish Journal of Computer and Mathematics Education (TURCOMAT)***, 12(14), 5601-5611.

98. M. Abdullah and A. S. Mohammed, "TWO APPROACHES FOR LUNG COVID-19 INFECTION CLASSIFICATION ON CT IMAGE", In ***Int. Virtual Conf. Internet Things (IVCIT)***, Oxford, United Kingdom, 25th - 26th June, 2022, pp. 34–42, 2022.

RESUME

Mustafa Kamil ABDULLAH graduated first and elementary education in Baghdad-Iraq. He completed high school education at (Alsaydia High School) in Baghdad City after that in 2010 he started a bachelor's program in the Department of Department Software Engineering at Baghdad College of Economic Sciences University, He has worked in the computer field and is still in this work. He moved to Turkey and began studying for his master's education at the department of Computer Engineering at Karabuk University in the year 2020, His aim is to complete his doctoral studies, Insha'Allah.